minerals

Article

Rotation and Uplift of the Taoxi Dome and Its Implication for the Evolution of Wuyi Terranes in Cathaysia Block

Huan Liu [1,*], Wei Zhang [1] and Jinguo Zhang [2]

[1] China Geological Survey-Nanjing Center, Nanjing 210016, China
[2] School of Resources and Environment Engineering, Hefei University of Technology, Hefei 230009, China
* Correspondence: njliuhuan@mail.cgs.gov.cn

Abstract: The Taoxi dome stands out as a rotated-circular structure on maps of the Wuyi terrane, south China. The origin and tectonic activity analysis of the Taoxi dome is a window to understand the tectonic framework and aggregation process of the Wuyi terranes in the Cathaysia block. Our field observations demonstrated that two major phases of deformation, counterclockwise rotation and dome uplift, were recorded in the Taoxi dome. Geochronological data indicated that the counterclockwise rotation was initiated at about 422 Ma as a result of a sinistral slide collision between the North Wuyi terrane and the South Wuyi terrane along the Nanping–Ninghua tectonic belt during the Caledonian. Zircon dating ages of the intrusions developed in the Taoxi dome suggested that the Taoxi dome had undergone at least two strong upheavals and the uplift of the Taoxi dome was active during the periods 229–222 Ma and 158–100 Ma. Geochemical data indicated that the intrusions developed in the Taoxi dome had characteristics of high silica ($SiO_2 > 70$ wt.%) and belonged to the A2-type granites, which suggest that the Taoxi dome was long governed by a tectonic setting of post-collisional or anorogenic magmatism since the Caledonian. The strong movement of the Caledonian rotation and coeval strike-slip movement in the Wuyi terranes suggests that a slide rotation may have been a major characteristic in response to the rifting process of micro-terranes during the late Paleozoic in the Cathaysia block.

Keywords: counterclockwise rotation; south China; Caledonian; Nanping–Ninghua tectonic belt; A-type granites

check for updates

Citation: Liu, H.; Zhang, W.; Zhang, J. Rotation and Uplift of the Taoxi Dome and Its Implication for the Evolution of Wuyi Terranes in Cathaysia Block. *Minerals* **2022**, *12*, 1267. https://doi.org/10.3390/min12101267

Academic Editor: Dominique Gasquet

Received: 6 September 2022
Accepted: 4 October 2022
Published: 8 October 2022

1. Introduction

Rotation is an important component of describing deformation. Originally, horizontal layered rocks can become inclined strata and can be rotated as a result of faulting and folding processes. There are a number of reports of rotation at the plate and regional tectonic scales [1–15]. Tectonic rotation can provide much useful information for the evolution of the terranes. Understanding the rotating processes and related deformation in the geological record is of first-order significance in understanding the tectonic evolution of tectonic belts and the amalgamation of terranes.

The Wuyi terrane, developed as terrane in the Cathaysia block (Figure 1), was one of the most intensively researched areas to understand the evolution of the Cathaysia block [16]. The Taoxi dome stands out as a rotated-circular structure. The origin and tectonic activity analysis of the Taoxi dome is a window to understand the tectonic framework and aggregation process of the micro-terranes in the Cathaysia block. Detailed investigations and analyses of the well-exposed rotated-circular structure are essential and crucial for understanding the origin of the Taoxi dome. However, the timing and mechanism of the formation of the Taoxi dome remain controversial. The Taoxi dome was suggested as the name that includes the annular structure or circular structure and the widespread development of ring fracture system and related metallogenic belt [17,18]. Previous research suggested that the Taoxi dome was a metamorphic core complex developed mainly during the Indosinian movement in an extensional setting [19,20]. Chen et al. (2010) [21] proposed that the Taoxi dome exhibits characteristics of a metamorphic core complex but mainly uplift as a result of the intrusion of the asthenosphere and magmatism during the Yanshanian. Huang et al. (2018) [22] proposed that the Taoxi dome experienced multi-stages of uplift from the Caledonian to the Yanshanian for the multi-stage magmatism.

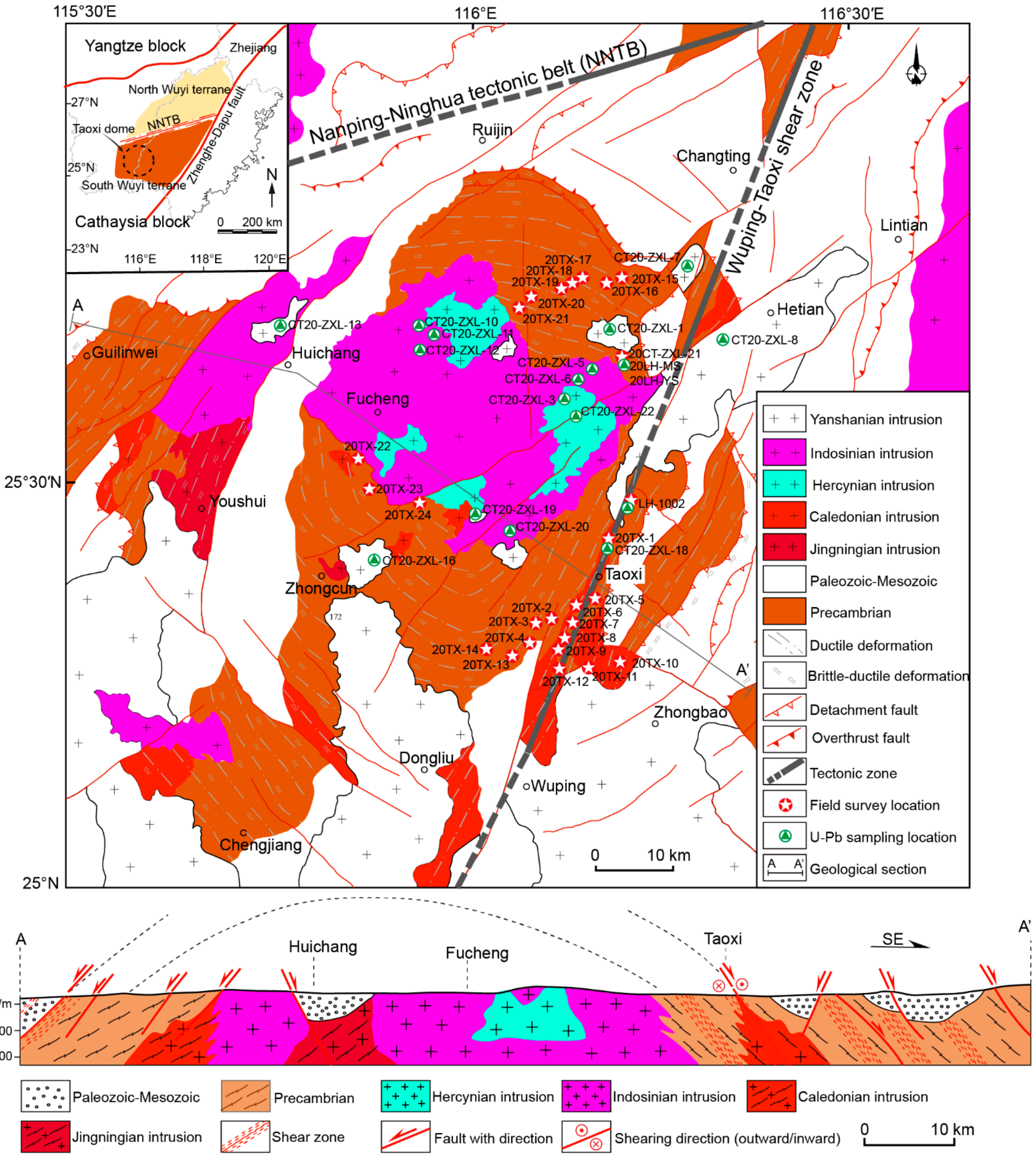

Figure 1. Simplified geological map of the Taoxi dome and the sampling locations. Note the tectonic setting of the Taoxi dome and the abbreviation of the Nanping–Ninghua tectonic belt (NNTB).

In this paper, we present structural, geochronological and geochemical data that show that the Taoxi dome has a counterclockwise rotation, and the rotated-circular structure is associated with the orogenesis within the Wuyi terranes during the Caledonian. Widespread deformation of the Precambrian basement and shear zones developed because of the counterclockwise rotation. Magmatism during the Indosinian and Yanshanian led to the main uplifting of the Taoxi dome, which accounts for the uplifting of the Precambrian basement in the South Wuyi terrane.

2. Geological Setting

It is generally believed that the Wuyi terranes rifted and moved away from the Cathaysia block on account of mantle magma upwelling since the Neoproterozoic [23–28]. The Wuyi terranes are composed of the North Wuyi terrane to the north and the South Wuyi terrane to the south, delineated by the Nanping–Ninghua tectonic belt (NNTB) with an approximately ENE–WSW strike (Figure 1) [29–34]. The Taoxi dome is situated in the South Wuyi terrane and is bounded by the Nanping–Ninghua tectonic belt (NNTB) to the north (Figure 1). The Wuping–Taoxi shear zone crosscuts the east part of the Taoxi dome in a SW–NE direction [35]. The Nanping–Ninghua tectonic belt was suggested to have been developed in an active continental margin setting with a strong deformation showing a sinistral sense of shear [30,32–34].

The Taoxi dome appears on maps as a metamorphic core complex, consisting of granitic intrusions in the core, surrounded by the circular deformed Precambrian basement of epimetamorphic rocks and Paleozoic to Mesozoic cover sediments.

The granitic intrusions are composed of diachronous magmatic rocks during these orogenic episodes in Jingningian (mainly in the Neoproterozoic), Caledonian (mainly in the Early Paleozoic), Hercynian (mainly in the Late Paleozoic), Indosinian (mainly in the Early Mesozoic) and Yanshanian (mainly in the Late Mesozoic). The Jingningian intrusions are locally developed and deformed in the western part of the Taoxi dome. The Caledonian intrusions have characteristics of widespread deformation with small-scale sporadic distribution in the Taoxi dome. The Hercynian and Indosinian intrusions are relatively concentrated with no deformation at the core of the Taoxi dome. The Yanshanian intrusions have a wide emplacement at the southeast part of the Taoxi dome.

The Precambrian basement is mainly composed of rock associations of low-grade metamorphosed sand–argillaceous flysch [19,22]. These low-grade metamorphosed sand–argillaceous rocks are mainly tectonic schist type in terms of deformation, including tectonic schist and tectonic gneiss. Circular ductile–brittle faults are common within the Precambrian basement at the surrounding part of the Taoxi dome.

Paleozoic to Mesozoic cover sediments were distributed around the Taoxi dome, of which the Early Paleozoic strata was suggested to be deposited in a back-arc basin setting [32]. Circular thrust and normal faults are common within the Paleozoic to Mesozoic cover sediments.

3. Field Observations and Microscopic Features

Our field observations and measurements were performed in the NE domain, the SW domain and the SE domain of the Taoxi dome, mostly in the Precambrian basement. The field characteristics of the Wuping–Taoxi shear zone were also investigated in detail.

Most parts of the Wuping–Taoxi shear zone can be observed in the field. The Wuping–Taoxi shear zone strikes NE at 20°–30°, dips toward the SE or NW at 30°–75° and extends along the eastern domain of the Taoxi dome for a distance of ~100 km, with a width of 2 to 10 km (Figure 1). The northern part of the shear zone developed in the Precambrian low-grade metamorphosed sand–argillaceous rocks and intersected with the Nanping–Ninghua tectonic belt (NNTB) to the north. The middle part lies between the batholith of the Taoxi dome and the Caledonian intrusions, whereas the southern part extends into the Caledonian intrusions and is locally invaded by the Yanshanian intrusions. The Wuping–Taoxi shear zone is characterized by protomylonite, mylonite and locally ultramylonite in felsic granites, and tectonic schist and tectonic gneiss in the Precambrian low-grade metamorphosed sand–argillaceous rocks. Foliations in the shear zone dip SE or NW at 30°–86° and are defined by aligned biotite and muscovite and by a serried mylonitic banding due to the flattening and alternation of quartzose, feldspathic and mica-rich porphyroclasts. Sub-horizontal mineral-stretching lineations, defined by linear aggregates of biotite, muscovite and quartz ribbons, are always present (Figures 2–8). Various shear sense indicators, including S-C fabrics, rotated quartz-feldspar porphyroclasts and quartz veins all suggest a dextral sense of shear in the Wuping–Taoxi shear zone (Figures 3 and 8a).

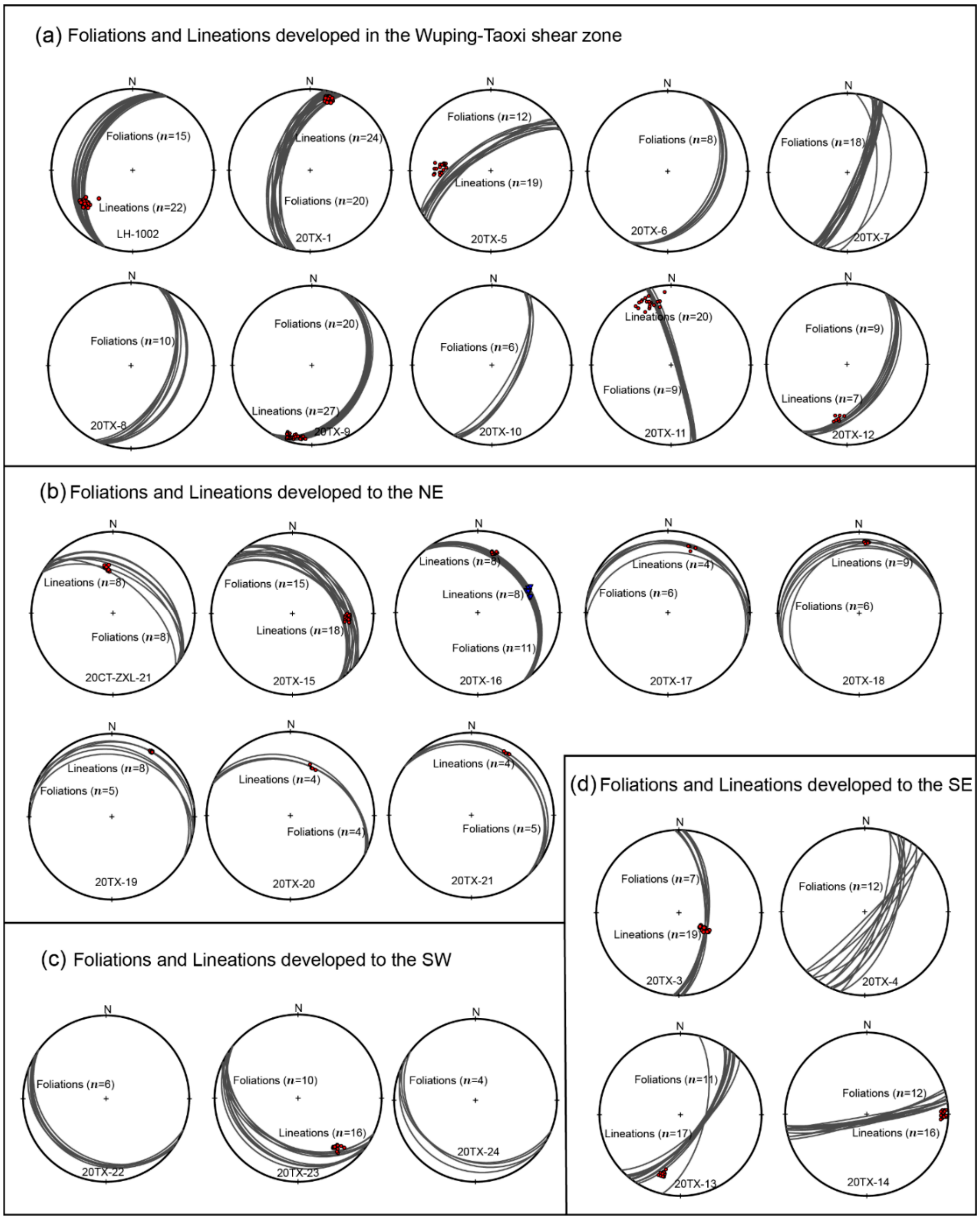

Figure 2. Lower-hemisphere, equal-angle stereograms of geometric fabrics in the Taoxi dome. (**a**) Geometric fabrics developed in the Wuping–Taoxi shear zone show NE-trending shear plane and sub-horizontal mineral stretching lineation. (**b**) Geometric fabrics developed in the northeastern part of the Taoxi dome show a NE-dipping shear plane and two groups of lineations, one of which downdip to the NE and another is NW–SE striking. (**c**) Geometric fabrics developed in the southwestern portion of the Taoxi dome show a SW-dipping shear plane and sub-horizontal mineral stretching lineation. (**d**) Geometric fabrics developed in the southeastern portion of the Taoxi dome show SE-dipping and two groups of lineations, one of which downdip to the SE and another is sub-horizontal.

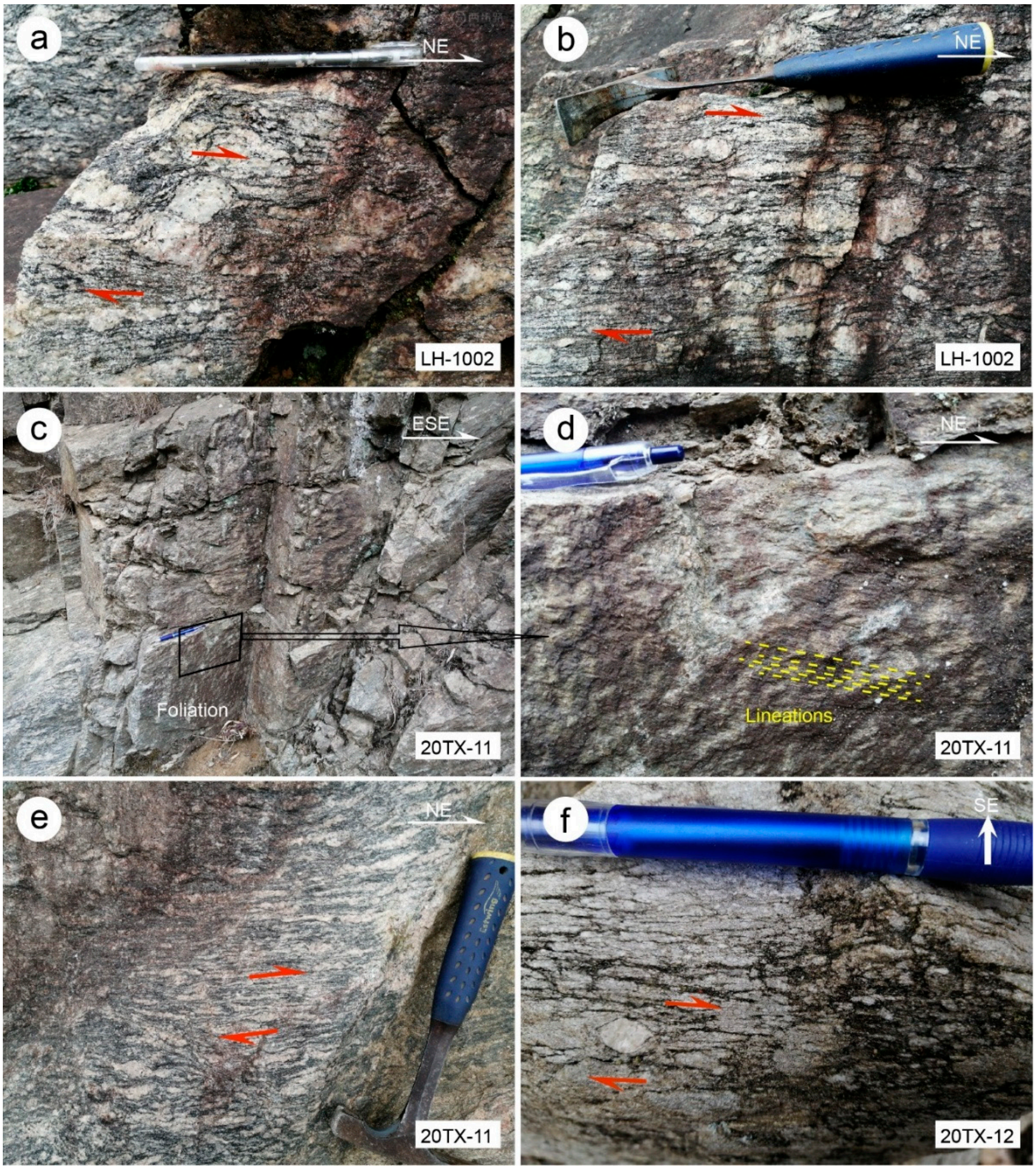

Figure 3. Outcrop photographs of structures in the Wuping–Taoxi shear zone. (**a**) Protomylonite in the Wuping–Taoxi shear zone, containing rotated quartz porphyroclasts that indicate a dextral sense of shear. (**b**) S-C fabrics and rotated quartz porphyroclasts demonstrate a dextral sense of shear. (**c**) Photograph showing high-angle shearing foliation in the Wuping–Taoxi shear zone. (**d**) Stretching lineations defined by elongate quartz and feldspar grains are approximately in a horizontal orientation. (**e**) Rotated feldspar porphyroclasts and S-C fabrics indicate a dextral sense of shear. (**f**) Rotated quartz porphyroclasts demonstrate a dextral sense of shear in the Wuping–Taoxi shear zone. The red arrows show the shear sense.

The NE domain of the Taoxi dome is occupied by pelitic–aleuritic metamorphic rocks and are intruded by granitoids and felsic dikes (Figures 1 and 4). The geometric fabrics developed in the NE domain of the Taoxi dome show a NE-dipping shear plane at 14°–60°, and two groups of lineations are found locally on the ductile shear plane, of which one group downdips to the NE and another is NW–SE striking (Figures 2b and 4). The closer to the core of the Taoxi dome, the flatter are the ductile shear planes. The linear fabrics are generally sub-horizontal in the core, whereas they are transposed into parallelism with the shear plane to the edge of the Taoxi dome (Figure 5a–d). Various shear sense indicators, including deformed dikes (Figure 5e), foliation fish (Figure 5f), S-C fabrics and rotated quartz-feldspar porphyroclasts (Figure 8b–e) demonstrate a sinistral sense of shear.

The SW domain of the Taoxi dome is characterized by the presence of mylonitized rocks, intruded by granites and surrounded by circular depositional basins (Figure 1). The mylonitized rocks developed SW-dipping shear planes with dips of 20° to 43° (Figure 2c). Stretching lineations defined by elongate quartz and feldspar grains are nearly sub-horizontal in the NW–SE direction (Figure 6a). Asymmetric intrafolial folds indicate a sinistral sense of shear in the SW domain of the Taoxi dome (Figure 6b). Microscopically, the S-C fabrics indicate a sinistral sense of shear (Figure 8f).

The SE domain of the Taoxi dome is occupied by biotite–plagioclase gneissic rocks and are intruded by Caledonian and Yanshanian granitoids and felsic dikes. The SE domain of the Taoxi dome is characterized by well-developed foliation and lineation, which resulted from the preferred orientation of the mineral grains in the Precambrian basement rocks. The NE-striking foliations dip steeply (>60°) to the SE and are defined by aligned biotite and plagioclase (Figure 2d). The moderately (~30°) SSW-plunging lineation is pronounced and is defined by linear aggregates of biotite, muscovite and quartz ribbons under the microscopic observation. Asymmetric intrafolial folds (Figure 7a) and boudins (Figure 7b) indicate a dextral sense of shear in the SE domain of the Taoxi dome.

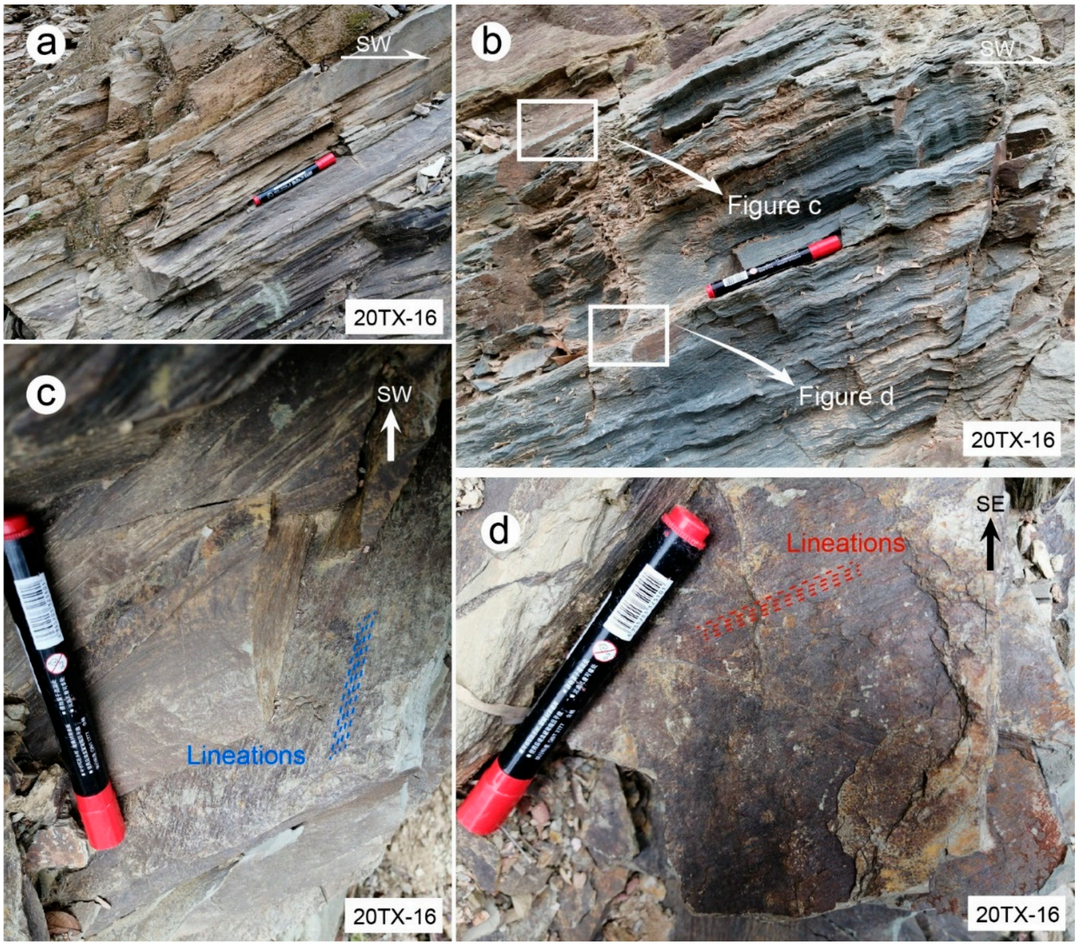

Figure 4. Outcrop photographs of structures in the NE domain of the Taoxi dome. (**a**) Felsic schist with NE-dipping foliations. (**b**) Undulating foliations developed in the felsic schist with two groups of stretching lineation. (**c**) One group of stretching lineation are downdip, photographed from above. (**d**) Another group of stretching lineation are foliation-parallel sub-horizontal, photographed from above.

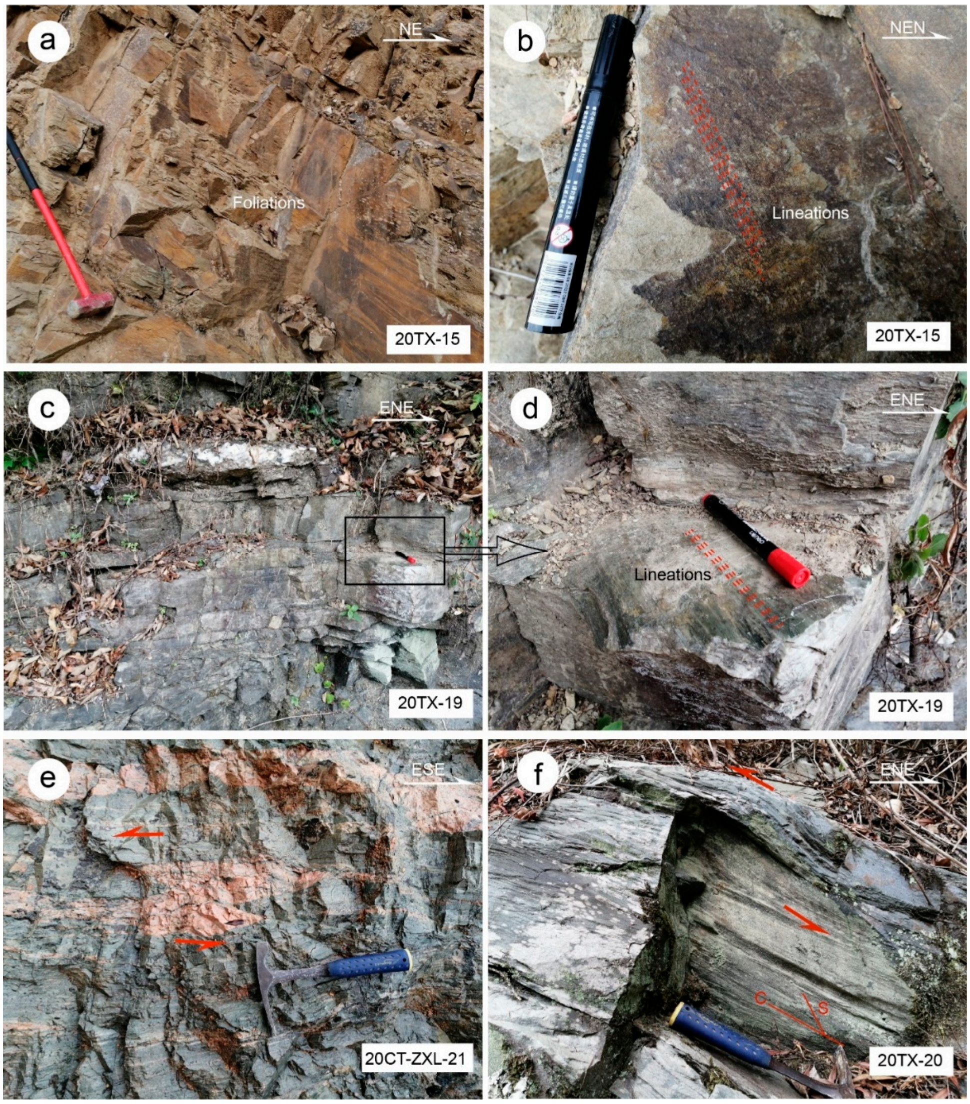

Figure 5. Outcrop photographs of structures at the NE–N domain of the Taoxi dome. (**a**) Felsic schist with NE-dipping foliations. (**b**) Stretching lineations developed. (**c**) Low-angle foliations. (**d**) Stretching lineations are downdip. (**e**) Syn-deformed dike indicates a sinistral sense of shear. (**f**) Foliation fish indicates a sinistral sense of shear. The red arrows show the shear sense.

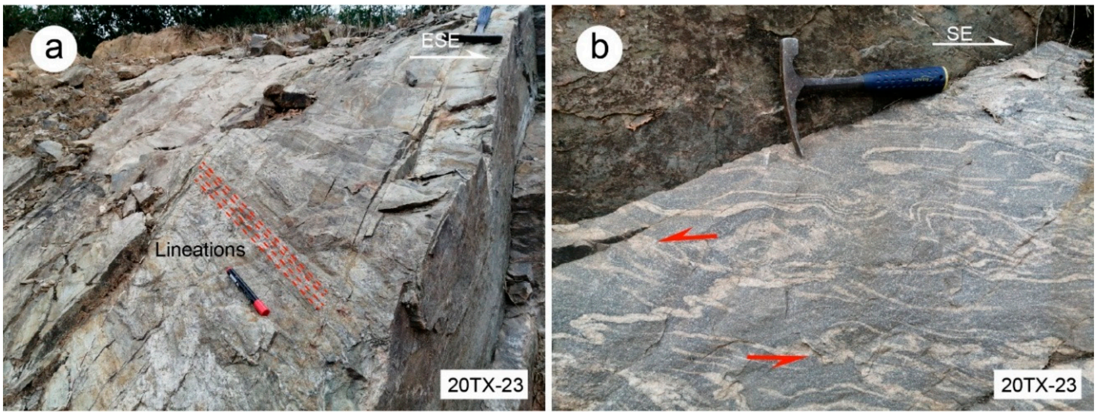

Figure 6. Outcrop photographs of structures in the SW domain of the Taoxi dome. (**a**) Mylonitized rock with SW-dipping foliations and NW–SE sub-horizontal stretching lineations. (**b**) Asymmetric intrafolial folds indicate sinistral sense of shear. The red arrows show the shear sense.

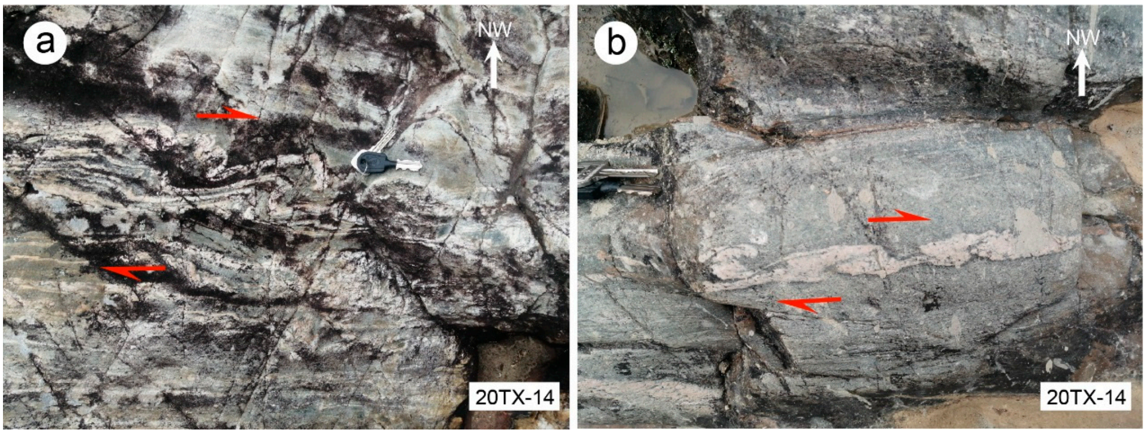

Figure 7. Asymmetric intrafolial folds (**a**) and boudins (**b**) in the SE domain of the Taoxi dome indicate a dextral sense of shear. The red arrows show the shear sense.

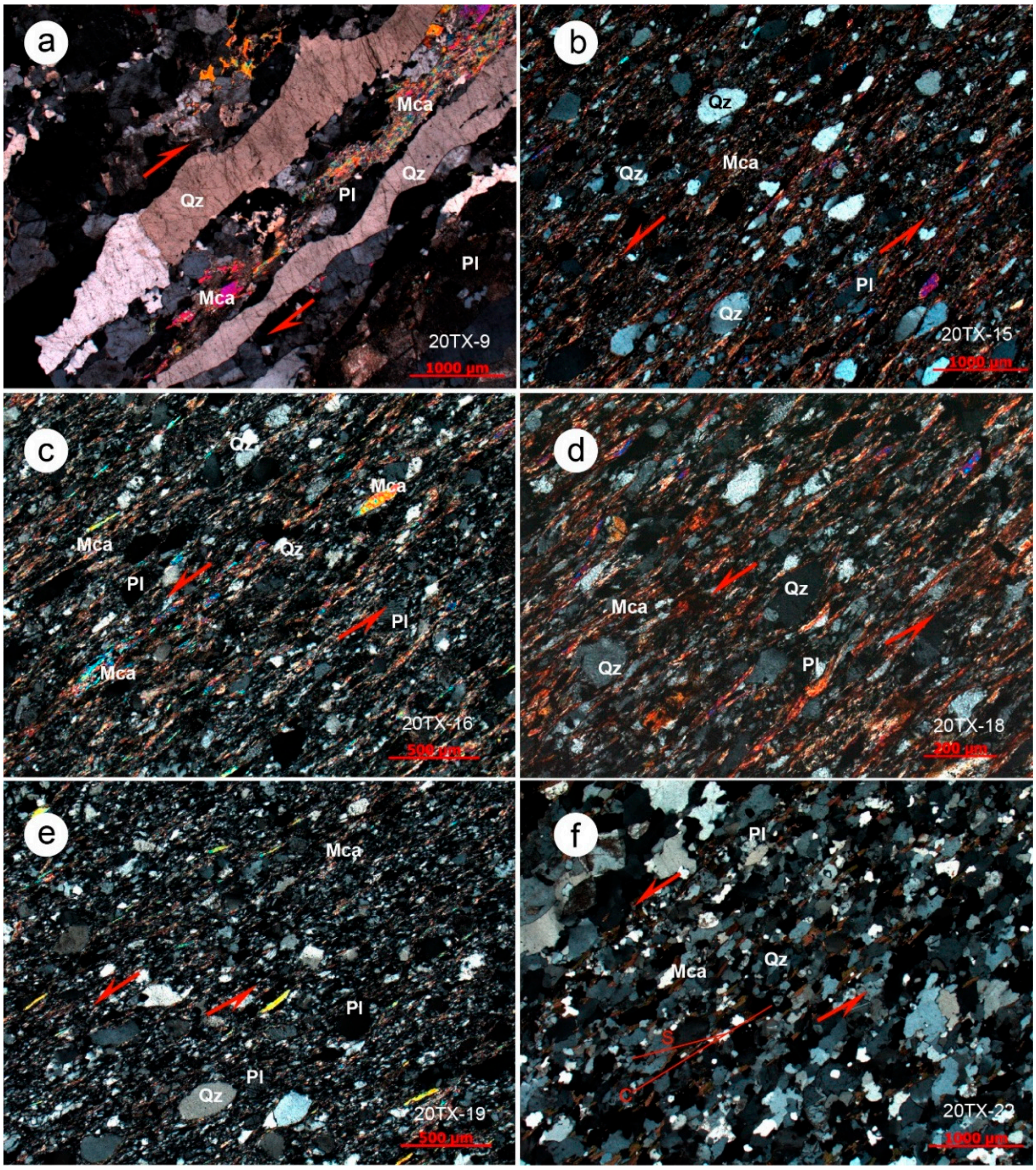

Figure 8. Photomicrographs of the deformed rocks in Taoxi dome. (**a**) Sample 20TX-9 collected from the Wuping–Taoxi shear zone. Note the strong elongated quartz grains and the strong alignment of

mica grains, asymmetrical banded-quartz fabric indicates a dextral sense of shear. (**b**–**e**) Samples collected from the NE–N domain of the Taoxi dome. Note the strong alignment of mica and quartz grains. The rotated quartz porphyroclasts and the S-C fabrics indicate a sinistral sense of shear. (**f**) Sample 20TX-22 collected from the SW domain of the Taoxi dome. Note the alignment of mica and quartz grains, and the S-C fabrics indicate a sinistral sense of shear. All were taken under cross-polarized light. Sample locations are noted in Figure 1. Qz = quartz, Pl = plagioclase and Mca = mica [36]. The red arrows show the shear sense.

4. Zircon U-Pb Geochronology

For the purpose of constraining the protolith and deformation age of the Taoxi dome, one sample of metasandstone, one sample of syn-deformed veins, one sample of undeformed granite and one sample of mylonitic granite were collected for zircon U-Pb dating. In order to analyze the effects of magmatism on the Taoxi dome, 14 samples of the intrusive rocks, practically covering the Taoxi dome, were collected for zircon U-Pb dating. The sampling locations are shown on Figure 1, for the sample descriptions see below and dating results are given in Supplementary Table S1.

4.1. Analytical Methods

Zircon grains were extracted from the samples using conventional techniques, which include crushing, sieving, heavy liquid separation and hand picking. The LA-ICP-MS U-Pb zircon analyses were performed at Hefei University of Technology, Hefei, China. Zircon grains were mounted on the surface of epoxy resin and were polished down to expose their centers. The internal structures of the zircons were revealed by cathodoluminescence (CL) imaging, which were taken by the Langfang Yuneng Rock Mineral Sorting Technology Service Co. LTD, Langfang, China. The ICP-MS used was Agilent 7500a and the Laser ablation system was ComPex102 ArF, manufactured by Coherent Inc., Mass, Waltham, America. The laser beam spot diameter for zircon analysis was 32 μm, with a repetition frequency of 6 Hz. Nist610 glass was used as the trace elements external standard. Standard zircon 91500 was used as an external standard for isotope fractionation correction. More details on the analytical procedure were described in Yan et al. (2012) [37]. The data were processed using ICPMSDataCal 18.0 (v7.8) [38,39]. Correction for common Pb followed the method of Andersen (2002) [40]. Concordia diagrams were produced using ISOPLOT (ver.4.15) [41]. The ages used in the following analyses were mostly between 90% and 100% concordant (Supplementary Table S1).

4.2. Geochronological Results

Sample 20LH-YS was an epimetamorphic sedimentary rock, interpreted to be a metasandstone. Zircons from the sample were mostly rounded-prismatic in shape, with grain sizes ranging from 50 to 100 μm. Some of the zircon grains showed well-developed oscillatory-zoned relict cores and oscillatory-zoned rims, whereas others showed light-grey planer-zoned mantles and dark homogeneous rims with oscillatory and sector zonation in the CL images (Figure 9a). Sixty LA-ICP MS spot analyses on these zircon grains were performed. The dating results showed that most zircon analyses were on or near the concordia curve (Figure 9a). The zircon spots had $^{206}Pb/^{238}U$ ages from 469 ± 14 Ma to 821 ± 23 Ma, with variable Th/U ratios from 0.22 to 2.14. The age distribution spectrum gave a single peak age at 731 Ma (Figure 9b).

Sample 20LH-MS was a K-feldspar vein, interpreted to be a syn-deformed vein cross-cutting the epimetamorphic sedimentary rocks as seen in Figure 5e. Zircons from the sample were mostly long and prismatic with an irregular shape, with the grain size varying from 100 to 200 μm (Figure 9c). The zircon grains showed well-developed bright oscillatory-zoned relict cores and dark oscillatory-sector zonation rims in the CL images. Thirty LA-ICP MS U-Pb analyses were carried out on this sample, mostly on the rims and partially on the cores. The age data can be grouped into two populations, of which most were plotted on or near the Concordia (Figure 9d). The oscillatory-zoned relict cores gave old $^{206}Pb/^{238}U$ ages older than 450 Ma with a relatively high Th/U ratio (>0.2), which are interpreted as the inherited zircon ages. The remaining analyses on the sector-zoned rims gave a range of $^{206}Pb/^{238}U$ ages from 337 ± 9 Ma to 444 ± 12 Ma with low Th/U ratios from 0.01 to 0.08, and most concordant analyses defined a weighted mean $^{206}Pb/^{238}U$ age of 422 ± 11 Ma (MSWD = 1.4) (Figure 9d). Based on the internal structure and the Th/U ratios of the zircon grains, we interpreted the age of 422 ± 11 Ma as the metamorphic–deformation age of the syn-deformed vein.

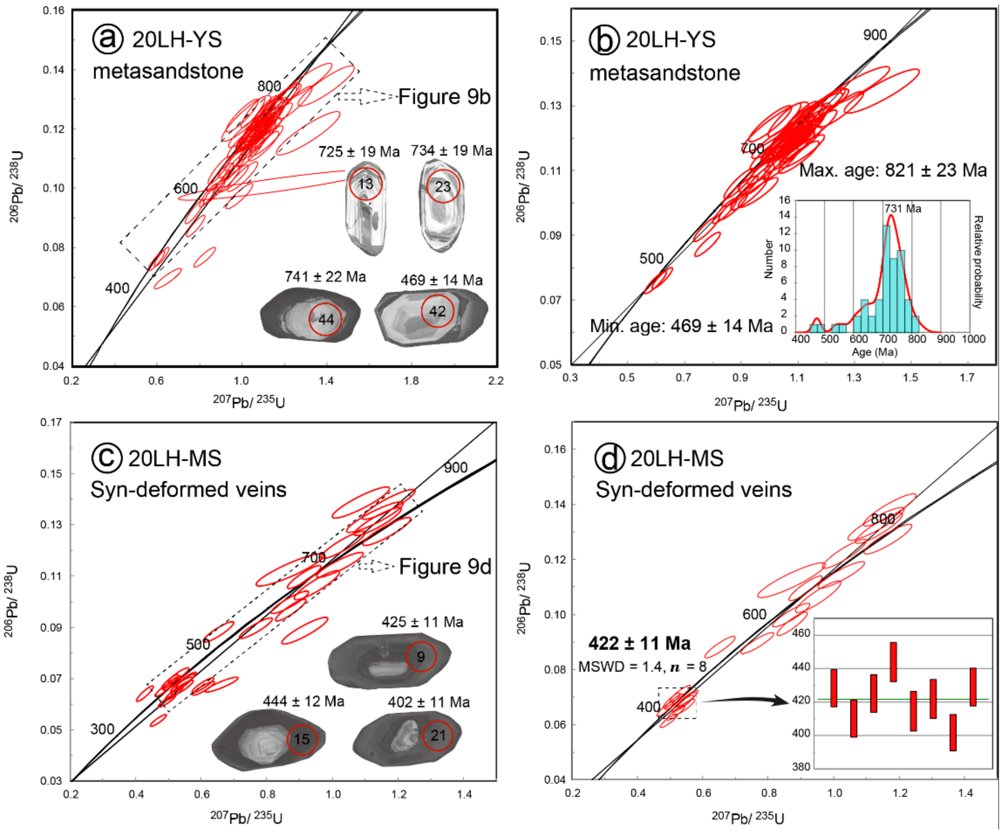

Figure 9. U-Pb Concordia diagrams for samples 20LH-YS (metasandstone) and 20LH-MS (syn-deformed veins). (**a**) Concordia diagram and representative CL images of sample 20LH-YS. (**b**) On or near the concordia curve diagram and age distribution spectrum of sample 20LH-YS. (**c**) Concordia diagram and representative CL images of sample 20LH-MS. (**d**) On or near the concordia curve diagram and weighted average age diagram of sample 20LH-MS.

Sample CT20-ZXL-18 was an undeformed granite, crosscut by the Wuping–Taoxi shear zone (Figure 1). Zircons from the sample were mostly long prismatic with a euhedral-subhedral shape, with the grain size varying from 100 to 300 μm. Their CL images showed oscillatory-zoned cores and oscillatory-zoned rims with a dark CL luminosity (Figure 10a). Thirty spot analyses on thirty zircon grains were performed. Removing the slightly discordant spots, most zircon analyses were on or near the concordant curve (*n* = 27). Three analyses on the cores of the zircons had Th/U ratios ranging from 0.1 to 0.2 and yielded $^{206}Pb/^{238}U$ ages of 567 ± 16 Ma, 592 ± 15 Ma and 1011 ± 25 Ma, which were interpreted as the inherited zircon ages. The remaining analyses on the oscillatory-zoned rims gave a range of $^{206}Pb/^{238}U$ ages from 411 ± 11 Ma to 456 ± 12 Ma with Th/U ratios from 0.08 to 0.71, defining a weighted mean $^{206}Pb/^{238}U$ age of 432 ± 5 Ma (MSWD = 0.9), which was interpreted as the emplacement age of the undeformed granite (Figure 10b).

Sample LH-1002 was a mylonitic granite developed in the Wuping–Taoxi shear zone (Figure 1). Zircons from the sample were prismatic in shape and were characterized by a large number of euhedral crystals, with the grain size varying from 100 to 200 µm. Most of the zircon grains showed an oscillatory-zoned core and rim in the CL images (Figure 10c). Twenty-five spot analyses were carried out on this sample, mostly on the rims. Removing one slightly discordant spot, most zircon analyses were on or near the concordia curve (*n* = 24). Two spots (spots 18 and 21) yielded $^{206}Pb/^{238}U$ ages of 495 ± 5 Ma (Th/U ratio = 0.2) and 946 ± 18 Ma (Th/U ratio = 0.15), respectively. The remaining analyses gave a range of $^{206}Pb/^{238}U$ ages from 411 ± 7 Ma to 430 ± 6 Ma with variable Th/U ratios from 0.04 to 0.42, defining a weighted mean $^{206}Pb/^{238}U$ age of 423 ± 2 Ma (MSWD = 0.75) (Figure 10d), which was interpreted as the emplacement age of the deformed granite.

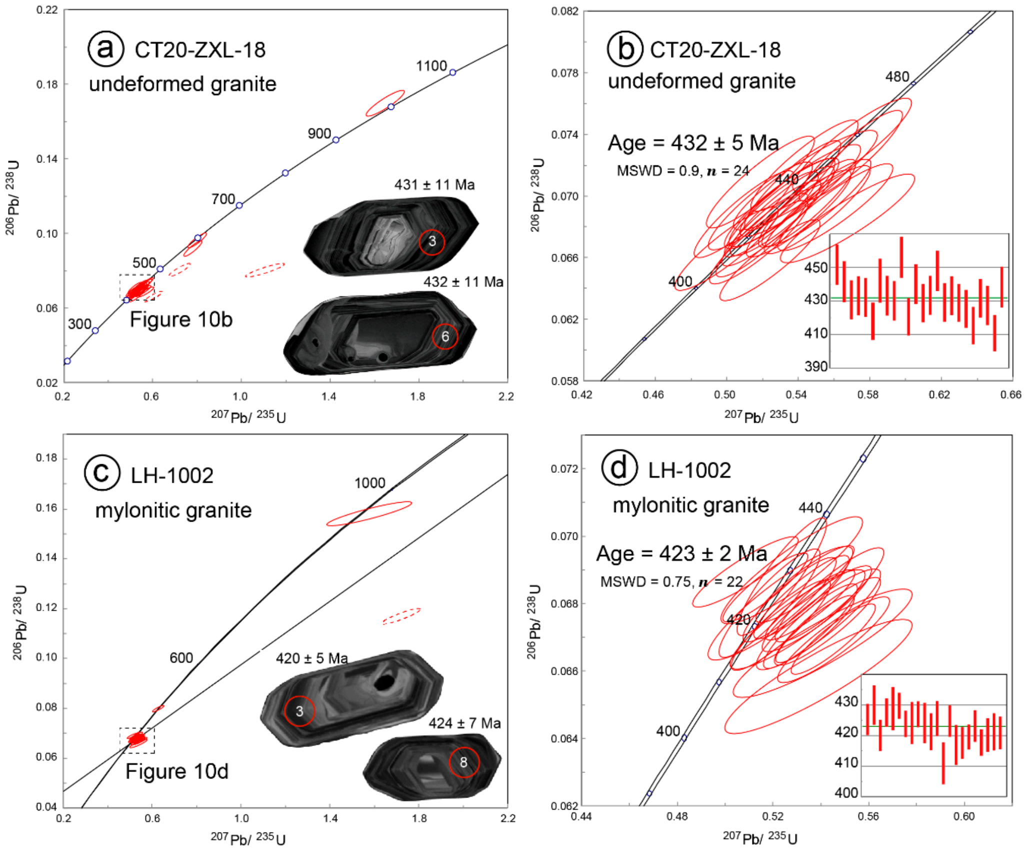

Figure 10. U-Pb Concordia diagrams for samples CT20-ZXL-18 (undeformed granite) and LH-1002 (mylonitic granite), which were developed in the Wuping–Taoxi shear zone. (**a**) Concordia diagram and representative CL images of sample CT20-ZXL-18. (**b**) Concordia diagram of the young ages and weighted average age diagram of sample CT20-ZXL-18. (**c**) Concordia diagram and representative CL images of sample LH-1002. (**d**) Concordia diagram of the young ages and weighted average age diagram of sample LH-1002.

The timing of the magmatic samples, widely developed in the Taoxi dome, were determined from the $^{206}Pb/^{238}U$ weighted mean age of the youngest group of the dated zircon grains. The youngest group of zircon grains had an igneous origin in all samples, as indicated by their idiomorphic to subhedral shapes, oscillatory zoning in CL images and high Th/U ratios (>0.2). The weighted mean ages for all the igneous zircons were interpreted to represent the timing of intrusion or the crystallization age for a particular sample. The dated zircon grains also included captured or inherited zircon that gave ages older than the youngest groups (Figures 11–13).

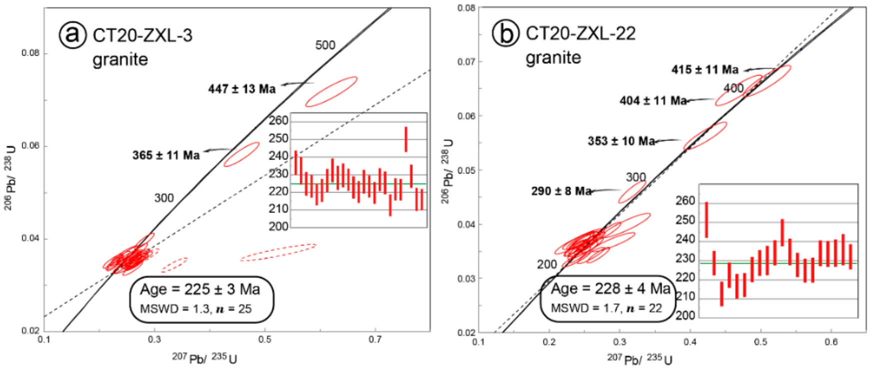

Figure 11. U-Pb Concordia diagrams for samples CT20-ZXL-3 (granite) and CT20-ZXL-22 (granite), which were sampled from the Hercynian intrusions in the Taoxi dome. (**a**) Concordia diagram and weighted average age diagram of sample CT20-ZXL-3. (**b**) Concordia diagram and weighted average age diagram of sample CT20-ZXL-22.

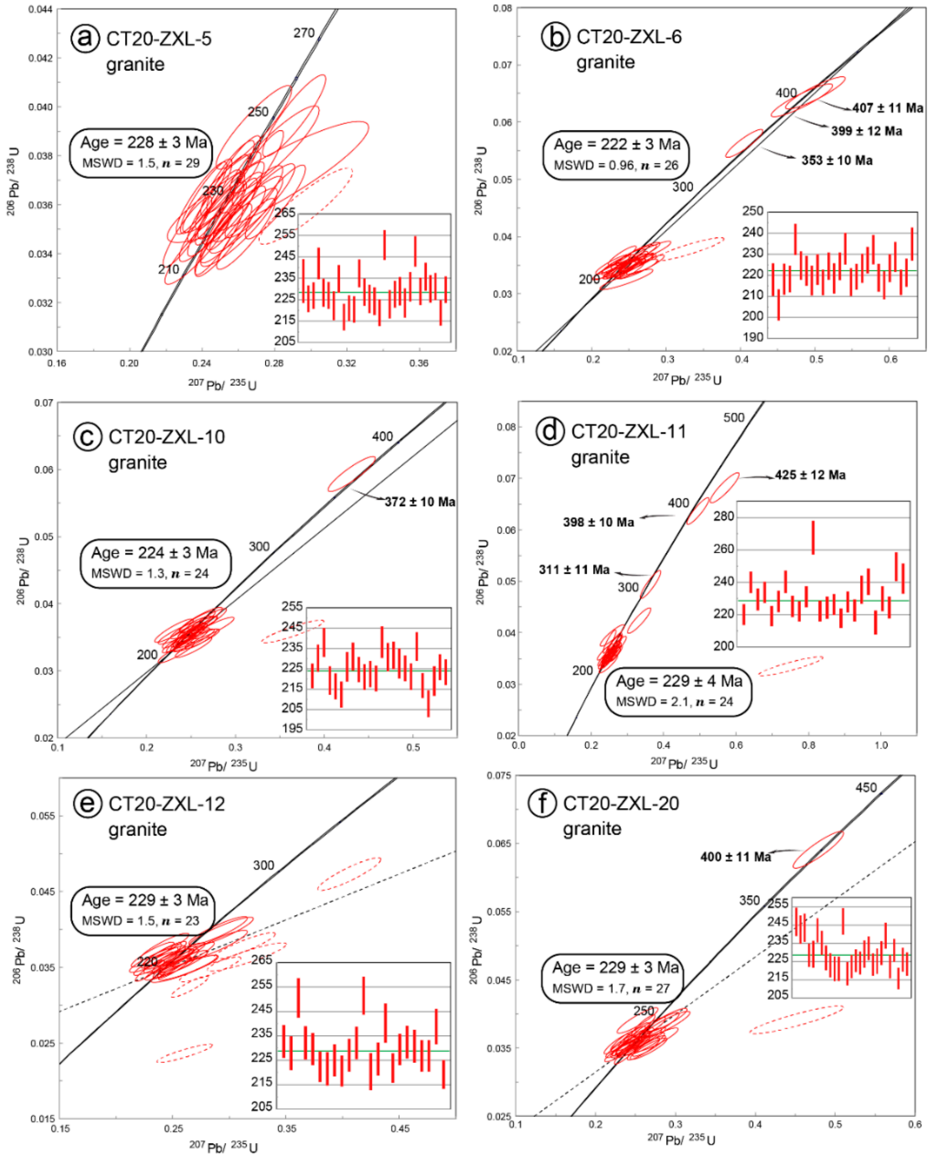

Figure 12. U-Pb Concordia diagrams for samples from Indosinian intrusions that have widespread development in the core of the Taoxi dome. (**a**) Concordia diagram and weighted average age diagram

of sample CT20-ZXL-5. (**b**) Concordia diagram and weighted average age diagram of sample CT20-ZXL-6. (**c**) Concordia diagram and weighted average age diagram of sample CT20-ZXL-10. (**d**) Concordia diagram and weighted average age diagram of sample CT20-ZXL-11. (**e**) Concordia diagram and weighted average age diagram of sample CT20-ZXL-12. (**f**) Concordia diagram and weighted average age diagram of sample CT20-ZXL-20.

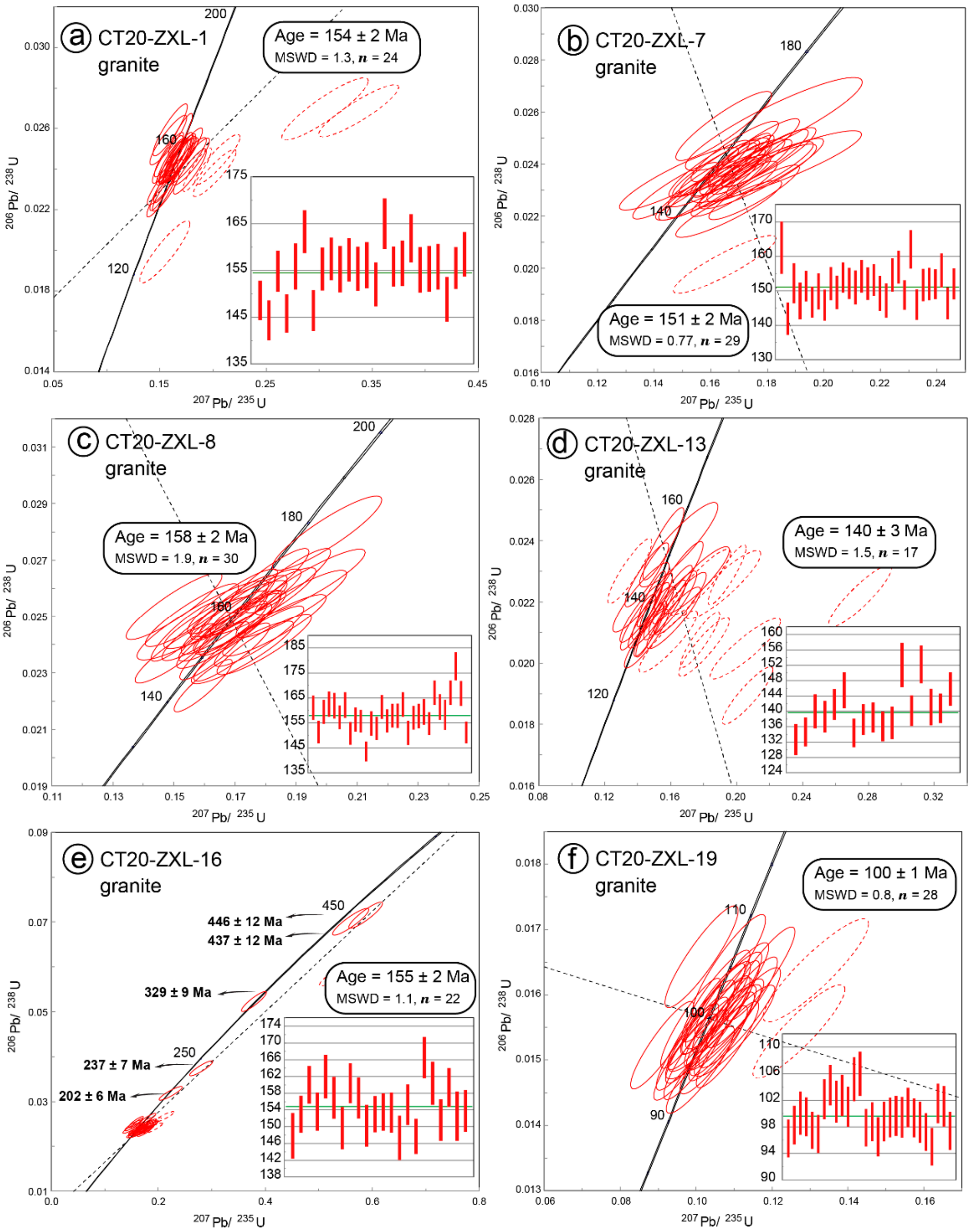

Figure 13. U-Pb Concordia diagrams for samples from the Yanshanian intrusions that developed around or in the Taoxi dome. (**a**) Concordia diagram and weighted average age diagram of sample CT20-ZXL-1. (**b**) Concordia diagram and weighted average age diagram of sample CT20-ZXL-7. (**c**) Concordia diagram and weighted average age diagram of sample CT20-ZXL-8. (**d**) Concordia diagram and weighted average age diagram of sample CT20-ZXL-13. (**e**) Concordia diagram and weighted average age diagram of sample CT20-ZXL-16. (**f**) Concordia diagram and weighted average age diagram of sample CT20-ZXL-19.

The two undeformed granitic samples, CT20-ZXL-3 (granite) and CT20-ZXL-22 (granite), considered to be Hercynian intrusions (Figure 1) [22], yielded $^{206}Pb/^{238}U$ weighted mean ages of 225 ± 3 Ma (Figure 11a) and 228 ± 4 Ma (Figure 11b), respectively. The two ages were interpreted to be intrusion ages. The Caledonian–Hercynian inherited zircon ages of 447 Ma to 290 Ma were also recorded in both of the two samples (Figure 11).

The six undeformed granitic samples from the Indosinian intrusions that developed in the core of the Taoxi dome yielded $^{206}Pb/^{238}U$ weighted mean ages of 228 ± 3 Ma (Figure 12a), 222 ± 3 Ma (Figure 12b), 224 ± 3 Ma (Figure 12c), 229 ± 4 Ma (Figure 12d), 229 ± 3 Ma (Figure 12e) and 229 ± 3 Ma (Figure 12f), respectively. The six ages were interpreted to be intrusion ages. The samples of CT20-ZXL-6, CT20-ZXL-10, CT20-ZXL-11 and CT20-ZXL-20 captured or inherited zircon ages from 353 Ma to 425 Ma (Figure 12).

Another batch of six undeformed granitic samples from the Yanshanian intrusions in the Taoxi dome yielded $^{206}Pb/^{238}U$ weighted mean ages of 154 ± 2 Ma (Figure 13a), 151 ± 2 Ma (Figure 13b), 158 ± 2 Ma (Figure 13c), 140 ± 3 Ma (Figure 13d), 155 ± 2 Ma (Figure 13e) and 100 ± 1 Ma (Figure 13f), respectively. The six ages were interpreted to be intrusion ages. The sample of CT20-ZXL-16 contained captured or inherited zircon ages from 202 Ma to 446 Ma (Figure 13).

5. Whole-Rock Geochemistry

5.1. Analytical Methods

The analysis of major elements and trace elements in the whole rock was completed at the National Research Center of Geoanalysis, China Geological Survey, Beijing, China. The major elements were analyzed with an X-ray fluorescence spectrometer (XRF), PW4400. The content of Fe was measured with an XRF to obtain the total Fe_2O_3 content, and the titration method was then used to determine the content of FeO. Finally, we obtained the content of Fe_2O_3 with the calculation formula of $Fe_2O_3 = TFe_2O_3\text{-}FeO \times 1.113$. The whole-rock trace element content was conducted by plasma mass spectrometry (PE300Q). The relative error of analysis accuracy conformed to the industrial standard of GB/T 14506.30-2010, GB/T 14506.28-2010, Q/GD 001-2002 (for Cr, Sb and Sn), GB/T 14506.2-2010 (for H_2O+), NY/T 86-1988 (for CO_2), LY/T 1253-1999 (for LOI) and GB/T 14506.14-2010 (for FeO).

5.2. Geochemical Results

The whole-rock geochemical data of 5 samples from the Caledonian intrusions, 12 samples from the Indosinian intrusions and 8 samples from the Yanshanian intrusions in the Taoxi dome are given in the Supplementary information (Table S2).

The Caledonian intrusions in the Taoxi dome had a moderate to high content of SiO_2 (68.62–81.75 wt.%), $Na_2O + K_2O$ (5.11–8.92 wt.%), K_2O (4.45–5.93 wt.%) and Ga (19.3–28.3 ppm). They were classified mainly as granites on the $(Na_2O + K_2O)\text{-}SiO_2$ diagram (Figure 14a) [42]. They displayed characteristics of high-K to shoshonitic rocks on the $K_2O\text{-}SiO_2$ diagram (Figure 14b). They belonged to peraluminous rocks on the A/NK-A/CNK diagram, with an A/NK of 1.22–1.83 and an A/CNK of 1.12–1.51 (Figure 14c). They belonged to the alkali-calcic to calc-alkalic series on the $(Na_2O + K_2O\text{-}CaO)\text{-}SiO_2$ diagram (Figure 14d) [43]. They displayed negative Ba, Nb, Ta, Sr, Eu and Ti anomalies and enrichment in Rb, Th, U and Pb on the primitive mantle normalized diagram (Figure 15a). They exhibited an enrichment of the LREEs and moderate to strong negative Eu anomalies with a $(La/Yb)_N$ ratio of 5.49–30.6 on the chondrite-normalized REEs patterns (Figure 15b). They had a high Ga/Al ratio (10,000 × Ga/Al = 2.58–5.28) and mainly belonged to the A-type granites on the $10,000 \times Ga/Al\text{-}K_2O + Na_2O$, $10,000 \times Ga/Al\text{-}(K_2O + Na_2O)/CaO$, $10,000 \times Ga/Al\text{-} K_2O/MgO$ and $10,000 \times Ga/Al\text{-}FeO/MgO$ diagrams (Figure 16) [44]. They also exhibited similar characteristics to the A-type granites on the plots of 10,000 × Ga/Al versus Zr, Nb, Ce and Y (Figure 17) [44]. On the tectonic discriminant diagrams of Rb/Nb-Y/Nb, Sc/Nb-Y/Nb and triangular plots, the Caledonian intrusions were mostly classified as A2 granitoids (Figure 18), which were emplaced in post-collisional tectonic settings and what may be true anorogenic magmatism [45].

The Indosinian intrusions in the Taoxi dome showed the typical features of the granites on the (Na_2O + K_2O)-SiO_2 diagram (Figure 14a), with a moderate-to-high content of SiO_2 (70.14–78.01 wt.%), high Na_2O + K_2O (7.01–9.46 wt.%) and Ga (15.0–27.0 ppm). They belonged to the high-K to shoshonitic series on the K_2O-SiO_2 diagram (Figure 14b), with a high content of K_2O (3.00–7.01 wt.%). They belonged to peraluminous rocks on the A/NK-A/CNK diagram, with an A/NK in the range of 1.20–1.41 and an A/CNK in the range of 0.95–1.39 (Figure 14c). They belonged to the alkali-calcic to calc-alkalic series on the (Na_2O + K_2O-CaO)-SiO_2 diagram (Figure 14d) [43]. They showed negative Ba, Nb, Ta, Sr, Eu and Ti anomalies and enrichment in Rb, Th, U and Pb on the primitive mantle normalized diagram (Figure 15c). They displayed an enrichment of the LREEs relative to the HREEs and moderate-to-strong negative Eu anomalies with a $(La/Yb)_N$ ratio of 0.73–13.81 on the chondrite-normalized REEs patterns (Figure 15d). They had high Ga/Al ratios (10,000 × Ga/Al = 2.26–3.73) and mainly belonged to the A-type granites on the 10,000 × Ga/Al-K_2O + Na_2O, 10,000 × Ga/Al-(K_2O+Na_2O)/CaO, 10,000 × Ga/Al-K_2O/MgO and 10,000 × Ga/Al-FeO/MgO diagrams (Figure 16) [44], and had a similar projection in the A-type granites field on the plots of 10,000 × Ga/Al versus Zr, Nb, Ce and Y (Figure 17) [44]. Almost all of the Indosinian intrusions belonged to the A2 granitoids on the tectonic discriminant diagrams of Rb/Nb-Y/Nb, Sc/Nb-Y/Nb and triangular plots (Figure 18) [45].

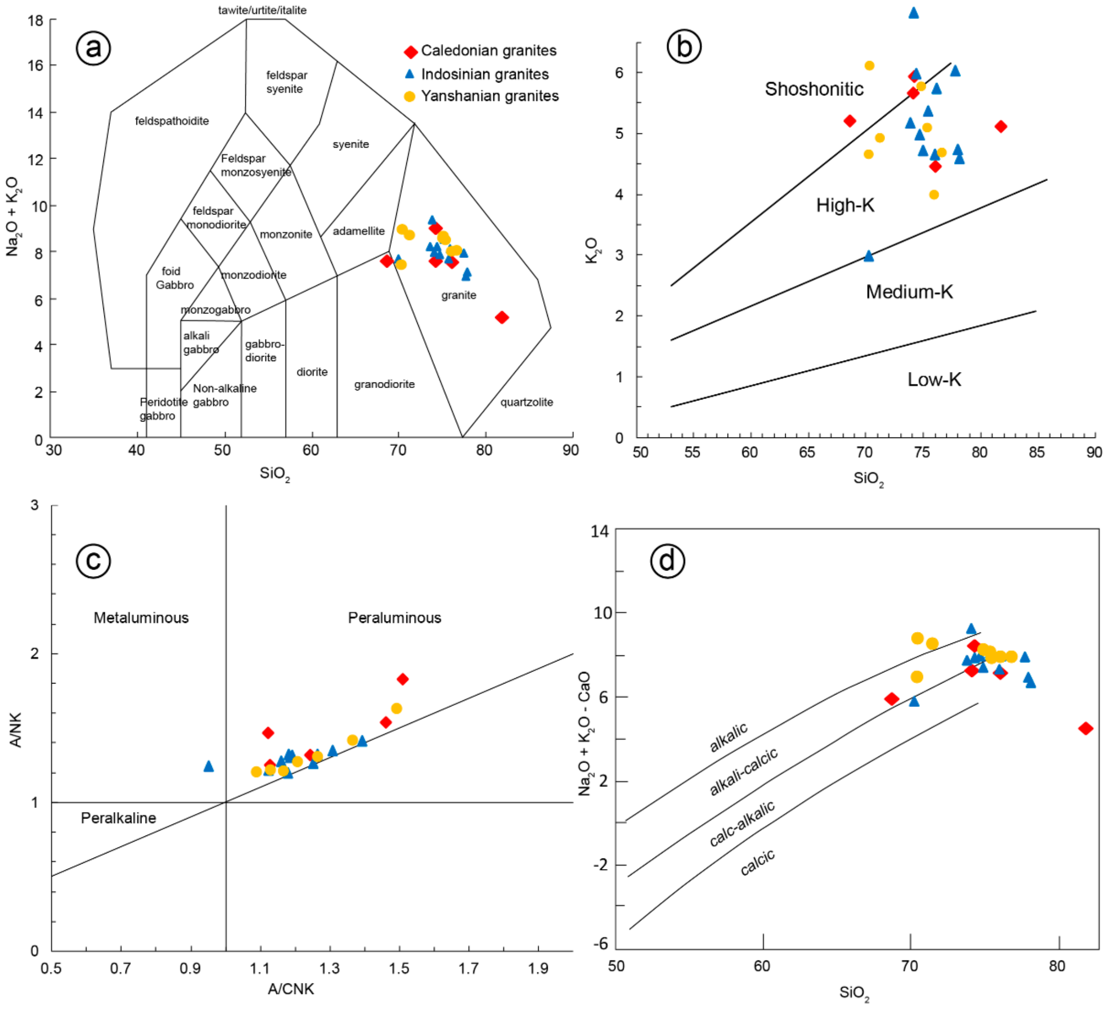

Figure 14. Plots of (**a**) Na_2O + K_2O versus SiO_2, (**b**) K_2O versus SiO_2, (**c**) A/NK [molar ratio Al_2O_3/(Na_2O + K_2O)] versus A/CNK [Al_2O_3/(CaO + Na_2O + K_2O)] [46] and (**d**) Na_2O + K_2O-CaO versus SiO_2 for the various granites from the Taoxi dome. The diagram in (**a**) is from Middlemost (1994) [42], (**d**) is from Frost et al. (2001) [43].

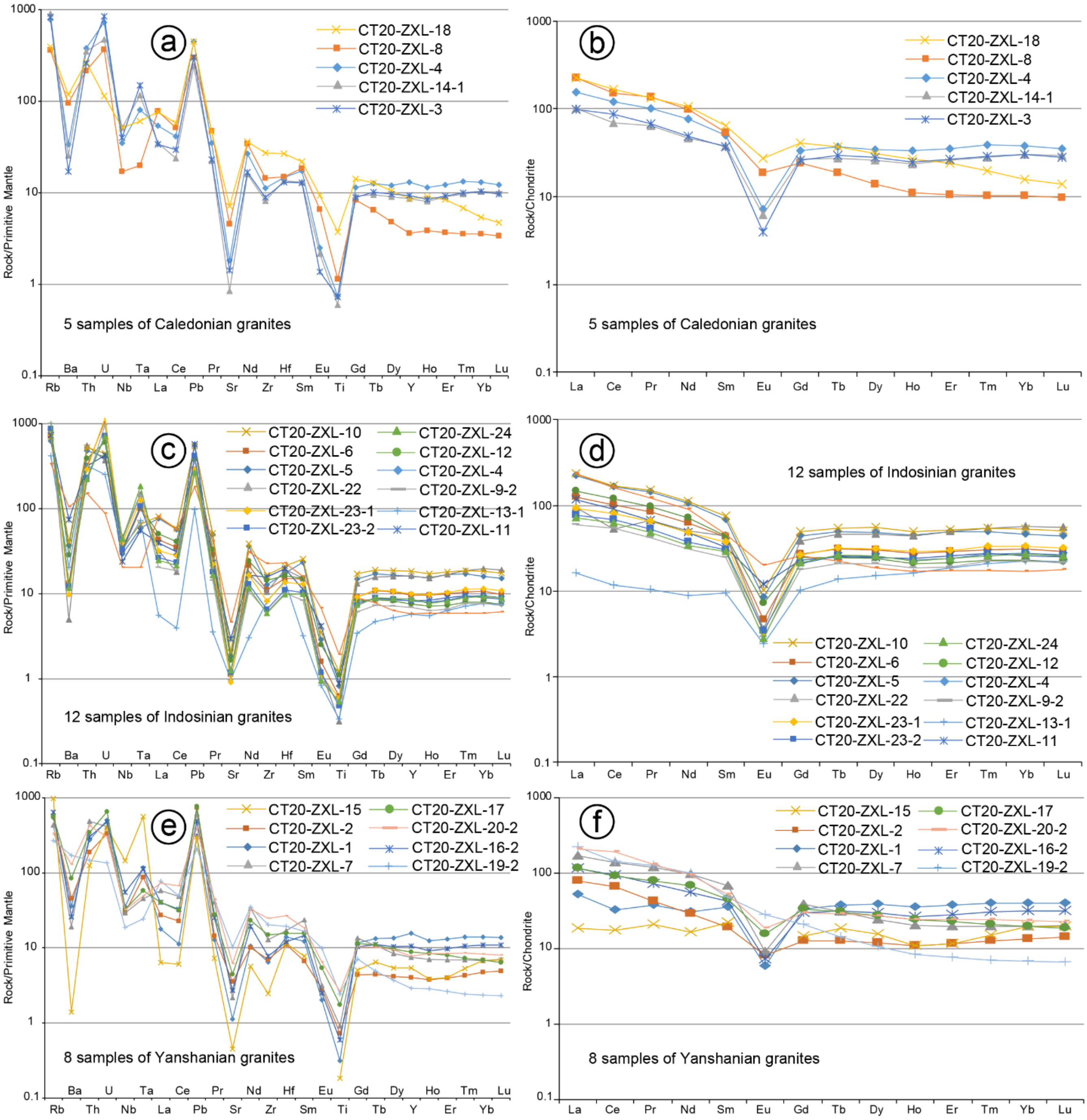

Figure 15. Primitive mantle-normalized trace element (**a**,**c**,**e**) and chondrite-normalized REE pattern (**b**,**d**,**f**) diagrams for the various granites form the Taoxi dome. The values of chondrite and primitive mantle are from Sun and McDonough (1989) [47].

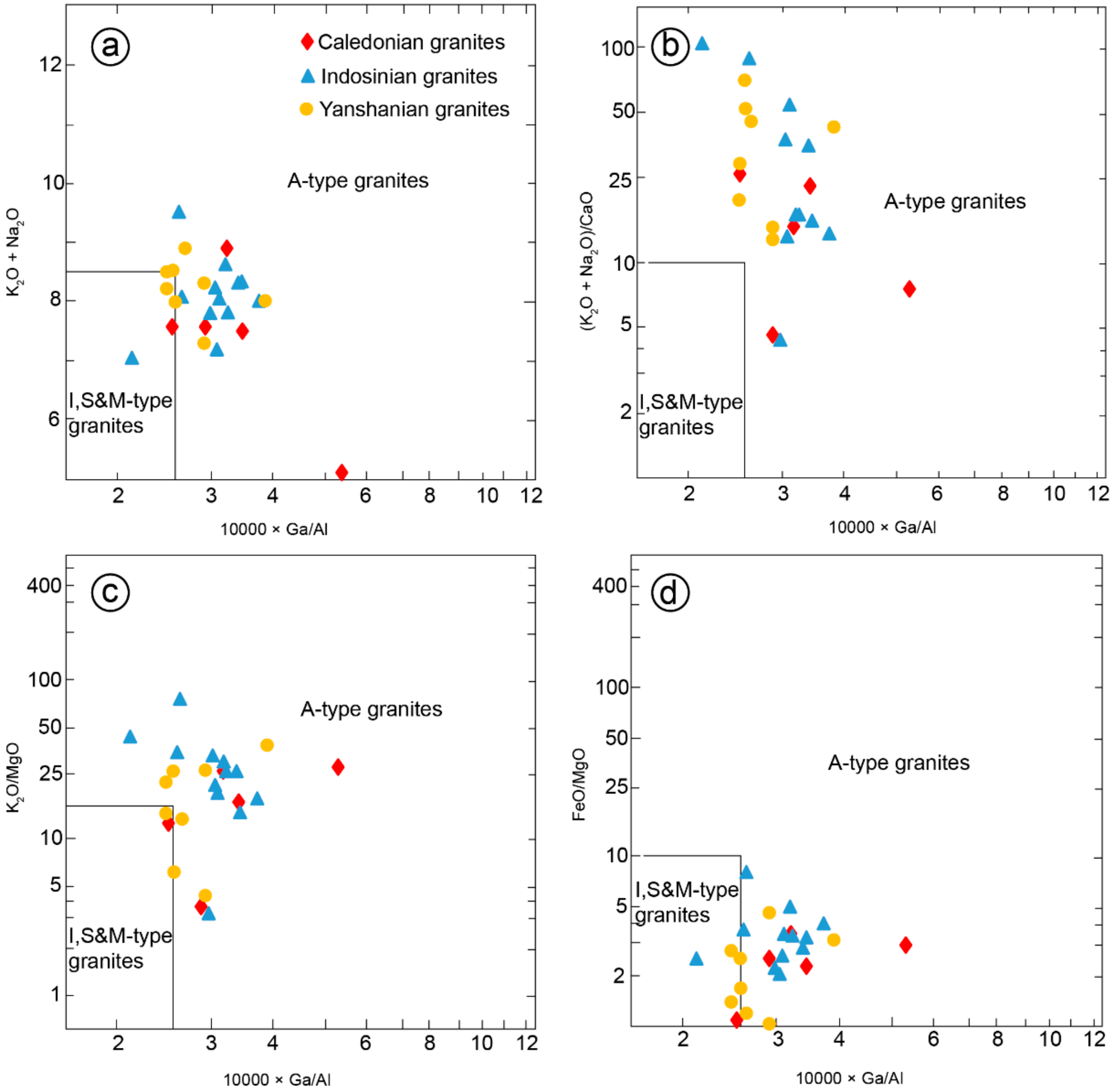

Figure 16. 10,000 × Ga/Al versus K_2O + Na_2O (**a**), (K_2O + Na_2O)/CaO (**b**), K_2O/MgO (**c**) and FeO/MgO (**d**) plots of various granites from the Taoxi dome. Diagrams are from Whalen et al. (1987) [44].

The Yanshanian intrusions had moderate-to-high SiO_2 content (70.32–76.67 wt.%), Na_2O + K_2O (7.34–8.87 wt.%), K_2O (3.99–6.11 wt.%) and Ga (17.3–29.4 ppm) and fell in the granitic series on the (Na_2O+K_2O)-SiO_2 diagram (Figure 14a). They mostly belonged to the high-K series on the K_2O-SiO_2 diagram (Figure 14b). They belonged to peralkaline rocks on the A/NK-A/CNK diagram, with an A/NK of 1.20–1.63 and an A/CNK of 1.09–1.50 (Figure 14c). They belonged to the alkali-calcic to alkalic series on the (Na_2O + K_2O-CaO)-SiO_2 diagram (Figure 14d) [43]. They showed negative Ba, Nb, Sr and Ti anomalies and enrichment in Rb, Th, U and Pb on the primitive mantle normalized diagram (Figure 15e). They displayed an enrichment of the LREEs relative to the HREEs and moderate to strong negative Eu anomalies on the chondrite-normalized REEs patterns (Figure 15f). They had moderate-to-high Ga/Al ratios (10,000 × Ga/Al = 2.48–3.93) and mainly belonged to the A-type granites on the 10,000 × Ga/Al-$K_2O + Na_2O$, 10,000 × Ga/Al-$(K_2O + Na_2O)/CaO$, 10,000 × Ga/Al-K_2O/MgO and 10,000 × Ga/Al-FeO/MgO diagrams (Figure 16) [44], and most of the data were projected into the A-type granites field on the diagrams of 10,000 × Ga/Al versus Zr, Nb, Ce and Y (Figure 17) [44]. The Indosinian intrusions mostly belonged to the A2 granitoids on the tectonic discriminant diagrams of Rb/Nb-Y/Nb, Sc/Nb-Y/Nb and triangular plots (Figure 18) [45].

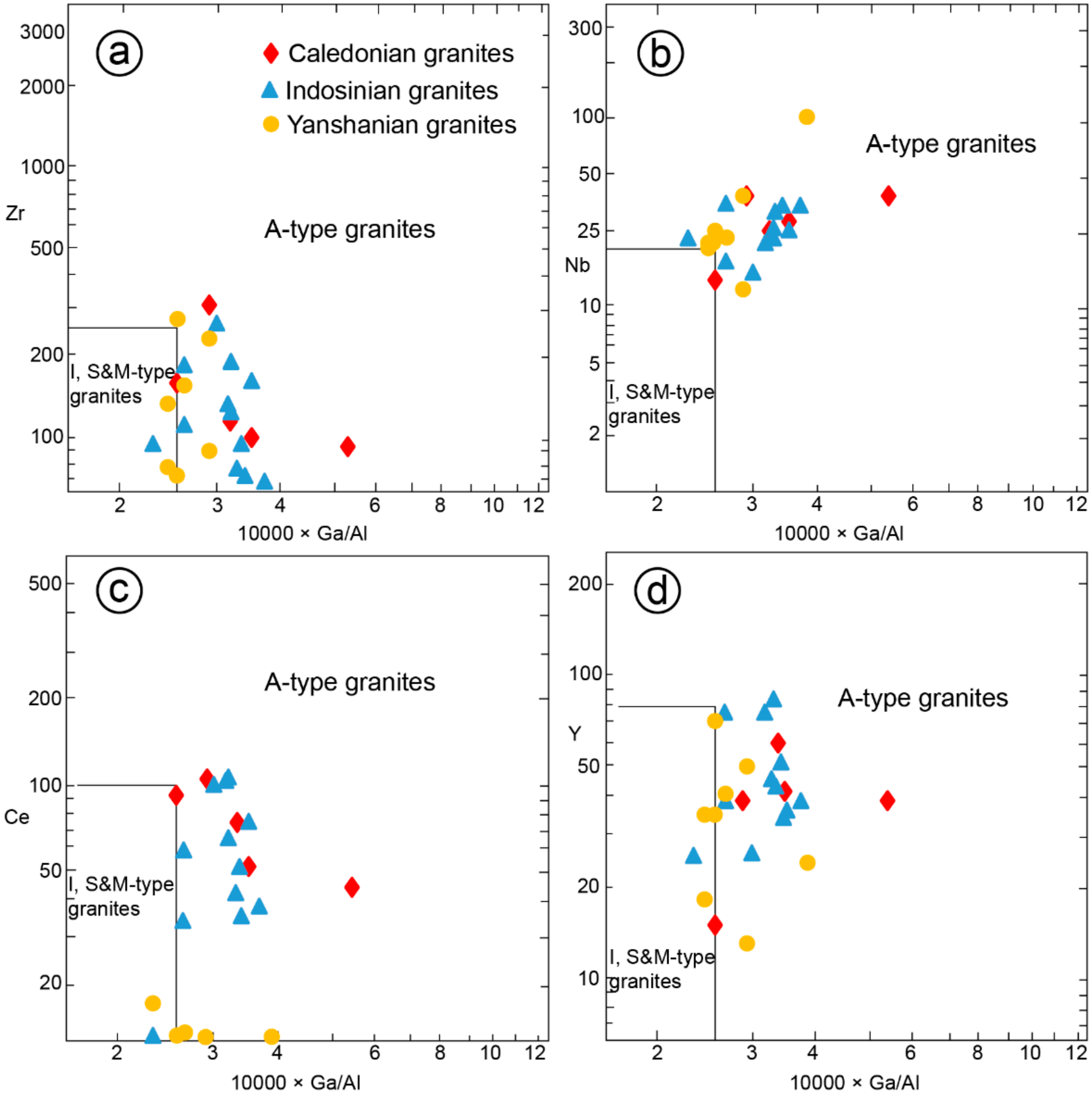

Figure 17. 10,000 × Ga/Al versus Zr (**a**), Nb (**b**), Ce (**c**) and Y (**d**) plots of various granites from the Taoxi dome. Diagrams are from Whalen et al. (1987) [44].

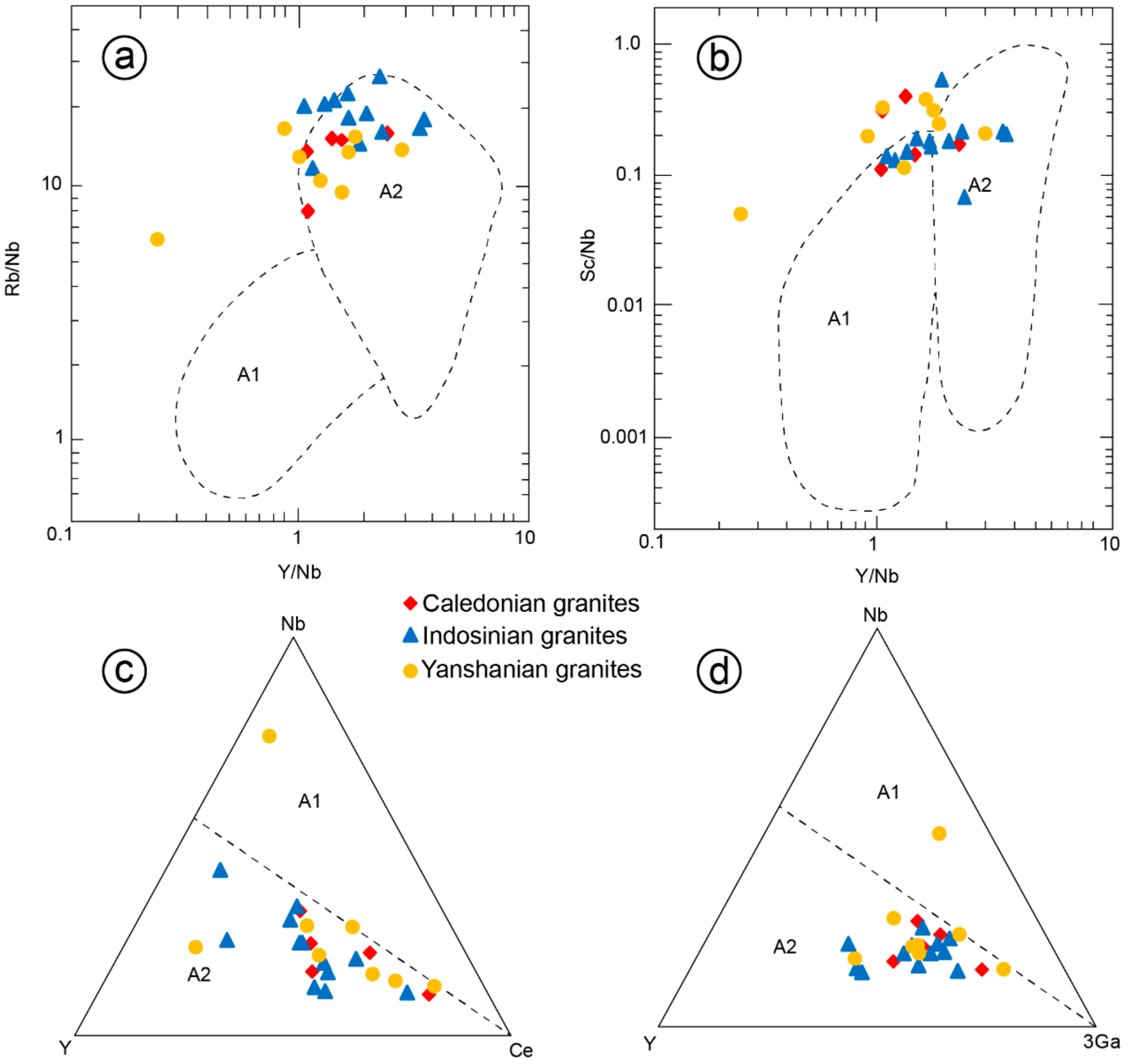

Figure 18. (**a**) Rb/Nb versus Y/Nb, (**b**) Sc/Nb versus Y/Nb plots for various A-type granites from the Taoxi dome. (**c**,**d**) are representative triangular plots for distinguishing between A1 and A2 granites in the Taoxi dome. Diagrams are from Eby (1992) [45].

6. Summary and Discussion

6.1. Timing of the Deformation in the Taoxi Dome

Our field observations demonstrated that two major phases of deformation were recorded by the kinematic indicators in the Taoxi dome. Movements along the Wuping–Taoxi shear zone were characterized by a strike-slip component with a dextral sense of shear, and along the NE–E domain of Taoxi dome it was sinistral with a dip-slip component. Along the SW domain of the Taoxi dome, it was sinistral, and along the SE domain of the Taoxi dome, it was dextral with a dip-slip component. Substantial strike-slip movement in the Taoxi dome was inferred to be a counterclockwise rotation (Figure 19a) and the dip-slip movement may have resulted in the uplift of the Taoxi dome.

The counterclockwise rotation mainly developed in the basement rocks and the Caledonian intrusive rocks. Therefore, the timing of the counterclockwise rotation occurred after the emplacement age of the basement rocks and the intrusion of the Caledonian batholith. The basement rocks that developed in the Taoxi dome were well dated at sample 20LH-YS (Figure 9) and gave zircon ages of 469–821 Ma, which showed a peak age at 731 Ma and constrained the provenance age of the basement rocks in the Taoxi dome. An undeformed but faulted granite in the Wuping–Taoxi shear zone, dated at sample CT20-ZXL-18, gave a date of 432 Ma. The above data indicated that the Taoxi dome experienced counterclockwise rotation after 432 Ma. A syn-deformed vein sample gave an age of 422 Ma, and one mylonitic granite sample in the Wuping–Taoxi shear zone gave a date of 423 Ma (Figure 10). These data suggest an activation of the counterclockwise rotation initiated at about 422 Ma (Figure 19a).

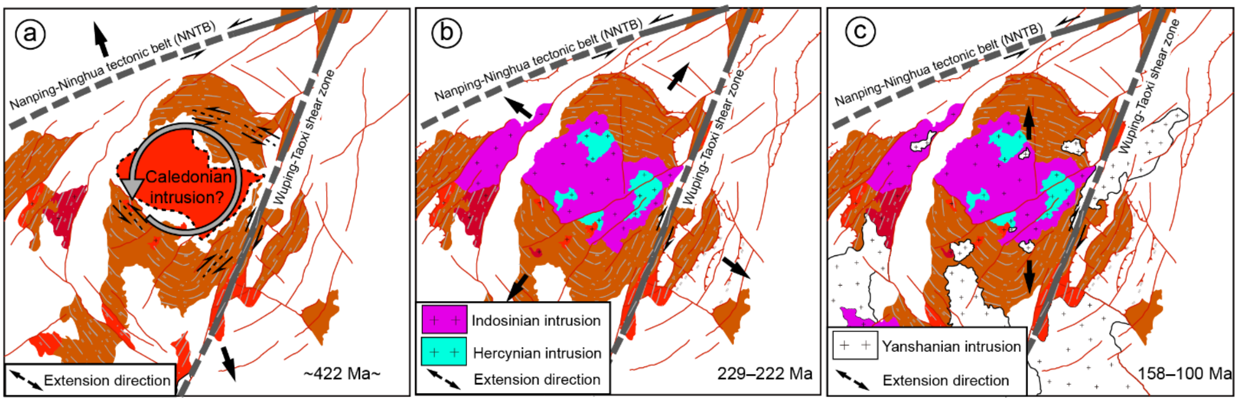

Figure 19. Simplified geological two-dimensional map showing the multi-stage evolution of the Taoxi dome. (**a**) Anticlockwise rotated deformation of the Precambrian basement in the Taoxi dome at about 422 Ma. (**b**) Widespread intrusion in the core of the Taoxi dome at 229–222 Ma. (**c**) Widespread intrusion around or in the Taoxi dome at 158–100 Ma.

Dip-slip movement and the widespread development of the intrusions in or around the Taoxi dome indicated that the Taoxi dome underwent strong uplift during magmatism. Undeformed granite in the Taoxi dome gave dates of 229–222 Ma and 158–100 Ma. These data suggest that the Taoxi dome underwent at least two strong upheavals and that the uplifting of the Taoxi dome was active during the period 229–222 Ma and 158–100 Ma (Figure 19b,c).

6.2. Origin and Tectonic Activity of the Taoxi Dome

The structures in the Taoxi dome showed a conspicuously counterclockwise rotation at about 422 Ma and it was bounded by the Nanping–Ninghua tectonic belt to the north (Figures 1 and 19). The Nanping–Ninghua tectonic belt was suggested to be a suture zone between the North Wuyi terrane and the South Wuyi terrane and was active during Caledonian orogeny times with a sinistral sense of shear, as proposed previously [34,48,49]. Similar geometrics and kinematics of shear zones were widely developed during the Caledonian in the Wuyi terranes [50–54]. The kinematic similarities and approximate deformation ages between the counterclockwise rotation of the Taoxi dome and the nearby boundary shear zones suggest their synchronous development and causal association.

High silica granites in general were suggested to possibly be extracted from an intermediate crystal mush into the shallow crust via the melt-crystal segregation process [55,56]. In this study, the Caledonian granites, Indosinian granites and Yanshanian granites that developed in the Taoxi dome showed geochemical characteristics of high silica ($SiO_2 > 70$ wt.%) and belonged to the A2-type granites, with similar geochemical features and isotopic compositions. These features suggest that the high silica A2-type granites that developed in the Taoxi dome were possibly derived from a common magma chamber via melt-crystal segregation in a tectonic setting of post-collisional or anorogenic magmatism during various orogenic events [45].

Combined with our field observations, chronological data and geochemical data, we propose that the Taoxi dome may have originally developed as a result of the strike-slip movement between the North Wuyi terrane and the South Wuyi terrane along the Nanping–Ninghua tectonic belt during the Caledonian (Figure 20a). The sinistral slide movement between the Wuyi terranes was responsible for the widespread rotation and ductile shearing in the Taoxi dome and may give rise to a Caledonian magmatism at the core of the Taoxi dome, as recorded in the magmatic and inherited zircons (Figures 11 and 12).

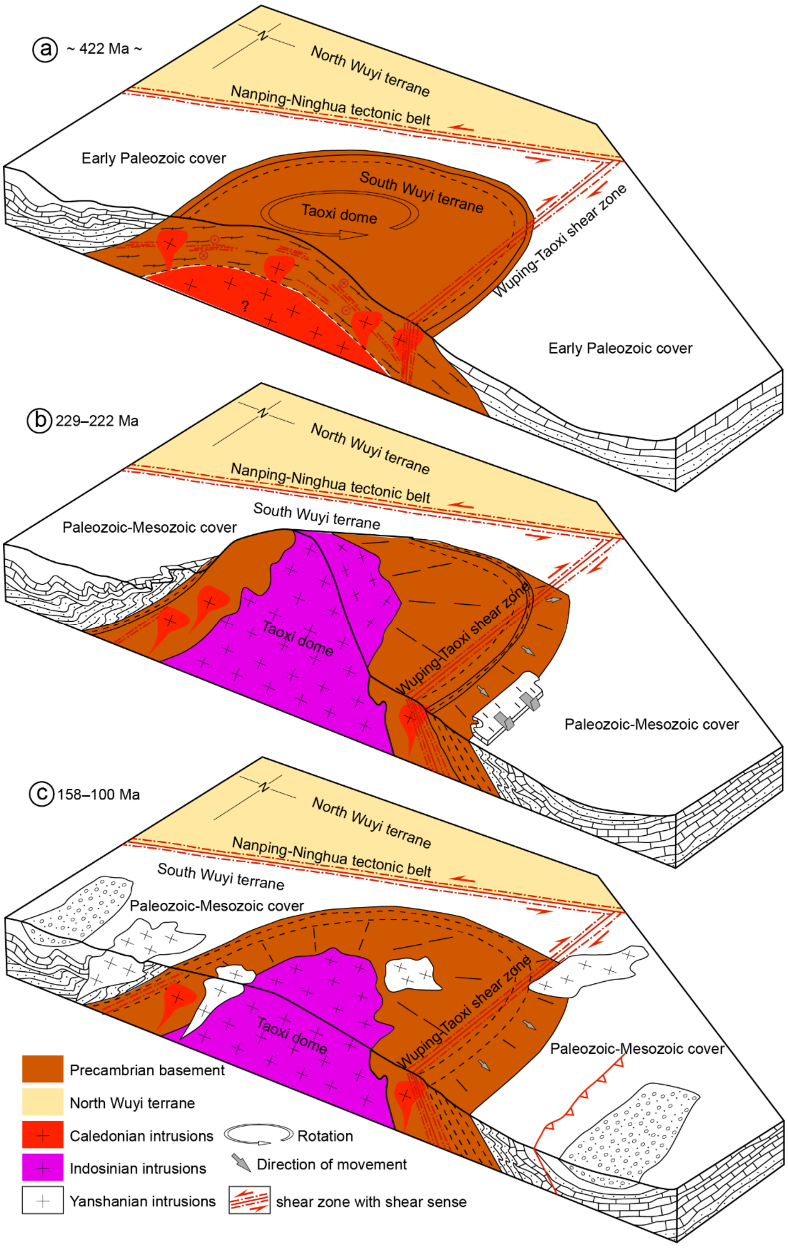

Figure 20. Simplified geological three-dimensional map showing the multi-stage uplift of the Taoxi dome. (**a**) Anticlockwise rotation of the Precambrian basement in the Taoxi dome at about 422 Ma, on account of collision between the North Wuyi terrane and the South Wuyi terrane along the Nanping–Ninghua tectonic belt, giving rise to the development of the Wuping–Taoxi shear zone and widespread deformation in the Precambrian basement. (**b**) Indosinian intrusions widely developed in the core of the Taoxi dome at 229–222 Ma, leading to the uplift of the Taoxi dome. (**c**) Yanshanian intrusions developed around or in the Taoxi dome at 158–100 Ma, which may have had an effect on the uplift of the Taoxi dome.

The magmatism during the Indosinian (229–222 Ma) may lead to the main uplifting of the Taoxi dome and result in the characteristics of a metamorphic core complex in the Taoxi dome (Figure 20b). The Yanshanian intrusions that developed around or in the Taoxi dome at 158–100 Ma may have an effect on the continued uplifting of the Taoxi dome (Figure 20c), of which the ages are consistent with the ages of the late Mesozoic volcanic rocks in southeast China [57].

6.3. Implication for the Evolution of Wuyi Terranes

Previous research suggested that the tectonic setting between the South Wuyi terrane and the North Wuyi terrane has been an aborted rift valley since the Neoproterozoic [58–60]. However, Jiang Y. et al. (2019, 2020) [30,31] proposed that the South Wuyi terrane and the North Wuyi terrane had not formed a unified Wuyi Block before 713 Ma. Some studies proposed that the collision of the two terranes occurred in the Caledonian [48,49].

The geochemical features of the high silica A2-type granites that developed in the Taoxi dome, including the Caledonian granites, Indosinian granites and Yanshanian granites, indicated that the tectonic evolution of the Taoxi dome was long governed by a tectonic setting of post-collisional or anorogenic magmatism since the Caledonian, and suggest that the South Wuyi terrane and the North Wuyi terrane had accomplished the collision before the Caledonian. Liu et al. (2021) [34] reported that widely Nanhua (756–720 Ma) island arc activity developed along the Nanping–Ninghua tectonic belt between the North Wuyi terrane and the South Wuyi terrane, which suggested that the South Wuyi terrane and the North Wuyi terrane had not collided during the Nanhua period. The detrital zircons in sample 20LH-YS have a peak age of 731 Ma, indicating that the provenance of the basement rocks in the Taoxi dome may have been derived from the Nanhua (756–720 Ma) island arc in the Nanping–Ninghua tectonic belt and that the South Wuyi terrane and the North Wuyi terrane must have been in close proximity to each other at that stage, which is possibly related to the compressional tectonic events during the Neoproterozoic (728–620 Ma) [61]. These features indicated that the aggregation time of the two terranes were constrained to the period between the Nanhua and Caledonian periods.

The counterclockwise rotation of the Taoxi dome indicated that the South Wuyi terrane showed an internal rotation deformation responding to the slide-shearing movement between the North Wuyi terrane and the South Wuyi terrane during the Caledonian, which is consistent with the widespread deformation at 460–420 Ma within the Wuyi terranes [16,53,55,62–64]. The Caledonian deformation in the Wuyi terranes has long been interpreted as a result of the intracontinental orogeny in the Cathaysia block [25,26,53,65,66]. However, Lin et al. (2018) [16] proposed that multi-terrane accretion-collision and large-scale strike-slip motions may be common features in the Cathaysia block, and that large-scale post-collisional rifting possibly occurred at the margins of the Wuyi terranes in the late Paleozoic. The rotation of the Taoxi dome, related to the slide movement between the Wuyi terranes during the Caledonian, was similar to the strike-slip motion of the micro-terranes in the Cathaysia block [16,67–69], indicating that the Caledonian slide-rotated rifting may have been one major deformation style in the tectonic evolution process in the Cathaysia block.

7. Conclusions

Our structural, geochronological and geochemical data for the Taoxi dome have led us to the following conclusions:

(1) Two major phases of deformation were recorded by the geometric and kinematic indicators in the Taoxi dome. They constituted a counterclockwise rotation and dome uplifting of the Taoxi dome.

(2) Zircon U-Pb dating of deformed rocks within the Taoxi dome constrained the timing of the counterclockwise rotation of the Taoxi dome to 422 Ma. Those of the intrusive rocks in the Taoxi dome showed features of A2-type granites and indicated that the uplifting of the Taoxi dome was active during the period 229–222 Ma and 158–100 Ma for the widespread magmatism at a post-collisional setting.

(3) The Caledonian A2-type granites that developed in the Taoxi dome suggest that the South Wuyi terrane and the North Wuyi terrane had accomplished the collision before the Caledonian. The original development of the Taoxi dome may have been a result of regional strike-slip rifting between the North Wuyi terrane and the South Wuyi terrane along the Nanping–Ninghua tectonic belt during the late Paleozoic (~422 Ma),

which suggests that a slide-rotated rifting may have been a major characteristic in the tectonic evolution of the micro-terranes in the Cathaysia block.

Supplementary Materials: The following supporting information can be downloaded at: https://www.mdpi.com/article/10.3390/min12101267/s1, Table S1 U-Pb isotope data for zircons; Table S2. Whole rock major and trace element data.

Author Contributions: Conceptualization, H.L.; methodology, H.L. and W.Z.; software, W.Z. and J.Z.; validation, H.L., W.Z. and J.Z.; formal analysis, J.Z.; investigation, H.L. and J.Z.; resources, H.L.; data curation, H.L.; writing—original draft preparation, H.L.; writing—review and editing, H.L.; visualization, H.L.; supervision, H.L.; project administration, H.L.; funding acquisition, H.L. All authors have read and agreed to the published version of the manuscript.

Funding: National Natural Science Foundation of China (grant #42002217) and the China Geological Survey (project #DD20190045).

Data Availability Statement: Not applicable.

Acknowledgments: This study was funded by the National Natural Science Foundation of China (grant #42002217) and the China Geological Survey (project #DD20190045). We appreciate the technical support from the U-Pb Laboratory of Hefei University of Technology (in particular, Quanzhong Li).

Conflicts of Interest: The authors declare no conflict of interest.

References

1. Jackson, J.; Molnar, P. Active faulting and block rotations in the western Transverse Ranges, California. *J. Geophys. Res.* **1990**, *95*, 22073–22089. [CrossRef]
2. Cocard, M.; Kahle, H.G.; Peter, Y.; Geiger, A.; Veis, G.; Felekis, S.; Paradissis, D.; Billiris, H. New constraints on the rapid crustal motion of the Aegean region: Recent results inferred from GPS measurements (1993–1998) across the West Hellenic Arc, Greece. *Earth Planet Sci. Lett.* **1999**, *172*, 39–47. [CrossRef]
3. Funahara, S.; Nishiwaki, N.; Miki, M.; Murata, F.; Otofuji, Y.; Wang, Y.Z. Paleomagnetic study of Cretaceous rocks from the Yangtze block, central Yunnan, China: Implications for the India-Asia collision. *Earth Planet Sci. Lett.* **1992**, *113*, 77–91. [CrossRef]
4. Funahara, S.; Nishiwaki, N.; Murata, F.; Otofuji, Y.; Wang, Y.Z. Clockwise rotation of the Red River fault inferred from paleomagenic study of Cretaceous rocks in the Shan-Thai-Malay Block of western Yunnan, China. *Earth Planet Sci. Lett.* **1993**, *117*, 29–42. [CrossRef]
5. Huang, K.N.; Opdyke, N.D. Paleomagnetic results from Cretaceous and Jurassic rocks of South and Southwest Yunnan: Evidence for large clockwise rotations in the Indochina and Shan-Thai-Malay terranes. *Earth Planet Sci. Lett.* **1993**, *117*, 507–524. [CrossRef]
6. Yang, Z.Y.; Besse, J. Paleomagnetic study of Permian and Mesozoic sedimentary rocks from Northern Thailand supports the extrusion model for Indochina. *Earth Planet Sci. Lett.* **1993**, *117*, 525–552. [CrossRef]
7. Yang, Z.Y.; Yin, J.Y.; Sun, Z.M.; Otofuji, Y.; Sato, K. Discrepant Cretaceous paleomagnetic poles between Eastern China and Indochina: A consequence of the extrusion of Indochina. *Tectonophysics* **2001**, *334*, 101–113. [CrossRef]
8. Wang, E.C.; Burchfiel, B.C. Interpretation of Cenozoic tectonics in the right-lateral accommodation zone between the Ailao Shan shear zone and the Eastern Himalayan syntaxis. *Int. Geol. Rev.* **1997**, *39*, 191–219. [CrossRef]
9. Wang, E.C.; Burchfiel, B.C.; Royden, L.H.; Chen, L.Z.; Li, W.X.; Chen, Z.L. Late Cenozoic Xianshuihe-Xiaojiang, Red River, and Dali Fault Systems of Southwestern Sichuan and Central Yunnan, China. *Geol. Soc. Am. Spec. Pap.* **1998**, *327*, 108.
10. Tanaka, K.; Mu, C.L.; Sato, K.; Takemoto, K.; Miura, D.; Liu, Y.Y.; Zaman, H.; Yang, Z.Y.; Yokoyama, M.; Iwamoto, H.; et al. Tectonic deformation around the eastern Himalayan syntaxis: Constraints from the Cretaceous paleomagnetic data of the Shan-Thai Block. *Geophys. J. Int.* **2008**, *175*, 713–728. [CrossRef]
11. Sato, K.; Liu, Y.Y.; Zhu, Z.C.; Yang, Z.Y.; Otofuji, Y. Paleomagnetic study of Middle Cretaceous rocks from Yunlong, Western Yunnan, China: Evidence of southward displacement of Indochina. *Earth Planet Sci. Lett.* **1999**, *165*, 1–15. [CrossRef]
12. Sato, K.; Liu, Y.Y.; Zhu, Z.C.; Yang, Z.Y.; Otofuji, Y. Tertiary paleomagnetic data from northwestern Yunnan, China: Further evidence for large clockwise rotation of the Indochina Block and its tectonic implications. *Earth Planet Sci. Lett.* **2001**, *185*, 185–198. [CrossRef]
13. Sato, K.; Liu, Y.Y.; Wang, Y.B. Paleomagnetic study of Cretaceous rocks from Pu'er, western Yunnan, China: Evidence of internal deformation of the Indochina Block. *Earth Planet Sci. Lett.* **2007**, *258*, 1–15. [CrossRef]
14. Otofuji, Y.; Tung, V.D.; Fujihara, M.; Tanaka, M.; Yokoyama, M.; Kitada, K.; Zaman, H. Tectonic deformation of the southeastern tip of the Indochina Peninsula during its southward displacement in the Cenozoic time. *Gondwana Res.* **2012**, *22*, 615–627. [CrossRef]
15. Tong, Y.B.; Yang, Z.Y.; Zhang, X.D.; Wu, Z.H.; Zhao, Y.; Wang, H.; Xu, Y.C.; Gao, L.; An, C.Z. The paleomagnetic analysis about the later Cenozoic crustal deformation characteristics of the Chuandian terrane clockwise rotation system in the southeast edge of Tibet Plateau. *Acta Geol. Sin.* **2014**, *88*, 2057–2070. (In Chinese with English abstract).

16. Lin, S.F.; Xing, G.F.; Davis, D.W.; Yin, C.Q.; Wu, M.L.; Li, L.M.; Jiang, Y.; Chen, Z.H. Appalachian-style multi-terrane Wilson cycle model for the assembly of South China. *Geology* **2018**, *46*, 319–322. [CrossRef]
17. Liu, L.Q. Taoxi annular structure and its controlling on the distribution of uranium deposit from the view of remote sensing image. *Geol. Jiangxi* **1996**, *10*, 69–74. (In Chinese with English abstract).
18. Chen, S.Z.; Huang, Z.Q.; Zhu, X.T.; Chen, G.; Ma, M. Magmatism and ore-forming background of the main deposits in Taoxi circular structure along the Wuyishan ore belt. *Geol. China* **2013**, *40*, 1569–1582. (In Chinese with English abstract).
19. Zhang, S.J.; Huang, C.Q.; Chen, Z.L.; Chen, J.L.; Chao, M.Z. Discussion on main features and formation mechanism of the convolutional structures of Taoxi metamorphic core complex in Wuyi mountains, South China. *Geol. Fujian* **2000**, *4*, 188–196. (In Chinese with English abstract).
20. Ma, J.Q. Discussion on some fundamental geology problems and their studying orientation, Fujian province. *Geol. Fujian* **2002**, *4*, 200–205. (In Chinese with English abstract).
21. Chen, S.Z.; Ma, M.; Chen, G.; Zhou, Y.; Zhu, X.T.; Qiu, J.L.; Mao, J.R. Taoxi uplift of Wuyi metallogenic belt, its tectonics, magmatism and metallogeny. *Earth Sci.-J. China Univ. Geosci.* **2010**, *35*, 969–984. (In Chinese with English abstract).
22. Huang, C.Q.; Zhang, K.B.; Shi, J.J.; Zhang, D.; Lin, Z.H.; Cheng, Q.; Zhao, J.X. Deformation characteristics and tectonic evolution of the Taoxi dome in southern Wuyishan on the boundary of Fujian and Jiangxi provinces. *East China Geol.* **2018**, *39*, 252–260. (In Chinese with English abstract).
23. Li, Z.X.; Li, X.H.; Kinny, P.D.; Wang, J.P.; Zhang, S.H.; Zhou, H.W. Geochronology of Neoproterozoic syn rift magmatism in the Yangtze Craton, South China and correlations with other continents: Evidence for a mantle super plume that broke up Rodinia. *Precambrian Res.* **2003**, *122*, 85–109. [CrossRef]
24. Li, X.H.; Li, Z.X.; Ge, W.C.; Zhou, H.W.; Li, W.X.; Ying, W.; Michael, T.D. Neoproterozoic granitoids in South China: Crustal melting above a mantle plume at ca. 825 Ma? *Precambrian Res.* **2003**, *136*, 51–66. [CrossRef]
25. Shu, L.S.; Faure, M.; Jiang, S.Y.; Yang, Q.; Wang, Y.J. SHRIMP zircon U-Pb age, litho-and biostratigraphic analyses of the Huaiyu Domain in South China-Evidence for a Neoproterozoic orogeny, not Late Paleozoic-Early Mesozoic collision. *Episodes* **2006**, *29*, 244–252. [CrossRef]
26. Shu, L.S.; Chen, X.Y.; Lou, F.S. Pre-Jurassic tectonics of the South China. *Acta Geol. Sin.* **2020**, *94*, 333–360. (In Chinese with English abstract).
27. Pan, G.T.; Lu, S.N.; Xiao, Q.H.; Zhang, K.X.; Yin, F.G.; Hao, G.J.; Luo, M.S.; Ren, F.; Yuan, S.H. Division of tectonic stages and tectonic evolution in China. *Earth Sci. Front.* **2016**, *23*, 10. (In Chinese with English abstract).
28. Zhang, J.K. A Mediterranean-style model for early Neoproterozoic amalgamation of South China. *J. Geodyn.* **2017**, *105*, 1–10. [CrossRef]
29. Zhao, X.L.; Xu, M.C.; Zhang, Y.J.; Jiang, Y.; Xing, G.F. New advances in the predevonian tectonic evolution of the Wuyi orogenic belt. *China Geol. Surv. Results* **2019**, *1*, 1–4. (In Chinese)
30. Jiang, Y.; Zhao, X.L.; Zhang, Y.J.; Xing, G.F.; Xu, M.C.; Liu, H. Neoproterozoic arc volcanic rocks of the Nanping-Ninghua tectonic belt, South China: Implications for the collision between the North and South Wuyi blocks. *Geol. J.* **2019**, *54*, 2679–2692. [CrossRef]
31. Jiang, Y.; Zhao, X.L.; Li, L.M.; Pan, G.T.; Xu, M.C.; Huang, W.C.; Liu, H. Neoproterozoic continental margin-arc magmatic activity of the Nanping-Ninghua tectonic belt, South China: Implications for tectonic evolution of the Wuyi orogenic belt. *Geol. China* **2020**, *47*, 1010–1024. (In Chinese with English abstract).
32. Jiang, J.; Xing, G.F.; Li, L.M.; Zhao, X.L.; Liu, H.; Zhang, J.G.; Li, J.H.; Wang, L.; Lu, K.J.; Wang, B. Age and provenance of Cambrian sequences in the Nanping-Ninghua-Ganzhou tectonic belt: Implication for tectonic evolution of the Cathaysia block. *Geol. J.* **2020**, *55*, 7057–7079. [CrossRef]
33. Liu, H.; Zhao, X.L.; Ge, Y.P.; Zhang, J.G.; Jiang, J.; Qin, X.Z. U-Pb dating of zircons from Xiayuan and Hongyegang intrusives in Dikou area and their geological significance. *Geol. Rev.* **2020**, *66*, 637–650. (In Chinese with English abstract).
34. Liu, H.; Zhao, X.L.; Zhang, J.G.; Jiang, J.; Yuan, H.W.; Wang, B.; Liu, M. The properties of Nanhua arc volcanic rocks in the Nanping-Ninghua tectonic belt of the Wuyi terranes and its implications for the integration of multi-micro-terranes in the Cathaysia block. *Acta Geol. Sin.* **2021**, *95*, 3629–3641. (In Chinese with English abstract).
35. Huang, C.Q. Deformation characteristics of Qili-Yongping ductile shear zone in Wuping county, Fujian province. *Geol. Fujian* **2002**, *1*, 46–52. (In Chinese with English abstract).
36. Laurence, N.W. IMA-CNMNC approved mineral symbols. *Mineral. Mag.* **2021**, *85*, 291–320.
37. Yan, J.; Peng, G.; Liu, J.M.; Li, J.M.; Li, Q.Z.; Chen, Z.H.; Shi, L.; Liu, X.Q.; Jiang, Z.Z. Petrogenesis of granites from Fanchang distinct, the Lower Yangtze region: Zircon geochronology and Hf-O isotopes constrains. *Acta Petrol. Sin.* **2012**, *28*, 3209–3227.
38. Liu, Y.S.; Hu, Z.C.; Gao, S.; Günther, D.; Xu, J.; Gao, C.G.; Chen, H.H. In situ analysis of major and trace elements of anhydrous minerals by LA-ICP-MS without applying an internal standard. *Chem. Geol.* **2008**, *257*, 34–43. [CrossRef]
39. Liu, Y.; Gao, S.; Hu, Z.; Gao, C.; Zong, K.; Wang, D. Continental and oceanic crust recycling-induced melt-peridotite interactions in the Trans-North China Orogen: U-Pb dating, Hf isotopes and trace elements in zircons of mantle xenoliths. *J. Petrol.* **2010**, *51*, 537–571. [CrossRef]
40. Andersen, T. Correction of common lead in U-Pb analyses that do not report ^{204}Pb. *Chem. Geol.* **2002**, *192*, 59–79. [CrossRef]
41. Ludwig, K.R. *Users Manual for Isoplot/Ex (rev.2.49): A geochronological toolkit for Microsoft Excel*; Berkeley Geochronolog Cente: Berkeley, CA, USA, 2001; Volume 1, pp. 1–58.
42. Middlemost, E.A.K. Naming materials in the magma/igneous rock system. *Earth-Sci. Rev.* **1994**, *37*, 215–224. [CrossRef]

43. Frost, B.R.; Barnes, C.G.; Collins, W.J.; Arculus, R.J.; Ellis, D.J.; Frost, C.D. A geochemical classification for granitic rocks. *J. Petrol.* **2001**, *42*, 2033–2048. [CrossRef]
44. Whalen, J.B.; Currie, K.L.; Chappell, B.W. A-type granites: Geochemical characteristics, discrimination and petrogenesis. *Contrib. Miner. Petr.* **1987**, *95*, 407–419. [CrossRef]
45. Eby, G.N. Chemical subdivision of the A-type granitoids: Petrogenetic and tectonic implications. *Geology* **1992**, *20*, 641–644. [CrossRef]
46. Pearce, J.A.; Harris, N.B.W.; Tindle, A.G. Trace element discrimination diagrams for the tectonic interpretation of granitic rocks. *J. Petrol.* **1984**, *25*, 956–983. [CrossRef]
47. Sun, S.S.; McDonough, W.F. Chemical and isotopic systematic of oceanic basalts: Implications for mantle composition and processes. *Geol. Soc. Spec. Publ.* **1989**, *42*, 313–345. [CrossRef]
48. Bian, X.Z.; Chu, Z.X.; Zhou, W.D. Framework of Palaeozoic-Mesozoic tectonic evolution of Fujian Province. *Geol. Fujian* **1993**, *12*, 280–291. (In Chinese with English abstract).
49. Wang, P.Z.; Chen, Y.A.; Cao, B.T.; Pan, J.D.; Wang, C.Y. Crust-upper-mantle structure and deep structural setting of Fujian province. *Geol. Fujian* **1993**, *12*, 79–158. (In Chinese with English abstract).
50. Shu, L.S. Predevonian tectonic evolution of South China: From Cathaysian block to Caledonian period folded Orogenic belt. *Geol. J. China Univ.* **2006**, *12*, 418–431. (In Chinese with English abstract).
51. Shu, L.S.; Deng, P.; Yu, J.H.; Wang, Y.B.; Jiang, S.Y. The age and tectonic environment of the rhyolitic rocks on the western side of Wuyi Mountain, South China. *Sci. China Earth Sci.* **2008**, *51*, 1053–1063. [CrossRef]
52. Shu, L.S.; Yu, J.H.; Jia, D.; Wang, B.; Shen, W.Z.; Zhang, Y.Q. Early Paleozoic orogenic belt in the eastern segment of South China. *Geol. Bull. China* **2008**, *27*, 1581–1593. (In Chinese with English abstract).
53. Shu, L.S.; Wang, B.; Cawood, P.A.; Santosh, M.; Xu, Z.Q. Early Paleozoic and early Mesozoic intraplate tectonic and magmatic events in the Cathaysia block, South China. *Tectonics* **2015**, *34*, 1600–1621. [CrossRef]
54. Li, J.H.; Zhang, Y.Q.; Zhao, G.C.; Stephen, T.S.; Dong, S.W.; Anthony, K.; Daniel, P.M.; Sun, H.S.; Wang, W.B.; Xin, Y.J. New insights into Phanerozoic tectonics of South China: Early Paleozoic sinistral and Triassic dextral transpression in the east Wuyishan and Chencai domains, NE Cathaysia. *Tectonics* **2017**, *36*, 819–853. [CrossRef]
55. Bachmann, O.; Bergantz, G.W. Rhyolites and their source mushes across tectonic settings. *J. Petrol.* **2008**, *49*, 2277–2285. [CrossRef]
56. Lee, C.T.A.; Morton, D.M. High silica granites: Terminal porosity and crystal settling in shallow magma chambers. *Earth Planet Sci. Lett.* **2015**, *409*, 23–31. [CrossRef]
57. Xu, X.B.; Zhang, Y.Q.; Jia, D.; Shu, L.S. U-Pb dating of volcanic rocks and granites along the Wuyishan belt: Constraints on timing of late Mesozoic tectonic events in southeast China. *Acta Geol. Sin.-Engl.* **2011**, *85*, 130–144.
58. Wei, D.G.; Jie, Y.J.; Huang, T.G. Regional geological structure of Fujian. *Reg. Geol. China* **1997**, *16*, 162–170. (In Chinese with English abstract).
59. Zhang, Q.L.; Lin, Y.Y.; Xu, S.Y.; Chen, J.S.; Du, J.M.; Ge, R.F. A new view on division of terranes and their tectonic evolution in Fujian province. *Resour. Surv. Environ.* **2008**, *29*, 168–176. (In Chinese with English abstract).
60. Li, X. Subdivision and characteristic of tectonic units in Fujian province. *Glob. Geol.* **2013**, *32*, 549–557. (In Chinese with English abstract).
61. Xu, X.B.; Zhang, Y.Q.; Shu, L.S.; Jia, D.; Wang, R.R.; Xu, H.Z. Precambrian geochronology and stratigraphy in the Wuyishan area, South China. *J. Stratigr.* **2010**, *34*, 254–267. (In Chinese with English abstract).
62. Faure, M.; Shu, L.S.; Wang, B.; Charvet, J.; Choulet, F.; Monie, P. Intracontinental subduction: A possible mechanism for the Early Palaeozoic Orogen of SE China. *Terra Nova* **2009**, *21*, 360–368. [CrossRef]
63. Charvet, J. The Neoproterozoic-Early Paleozoic tectonic evolution of the South China Block: An overview. *J. Asian Earth Sci.* **2013**, *74*, 198–209. [CrossRef]
64. Xu, X.B.; Zhang, Y.Q.; Shu, L.S.; Jia, D. La-ICP-MS U-Pb and ^{40}Ar/^{39}Ar geochronology of the sheared metamorphic rocks in the Wuyishan: Constraints on the timing of Early Paleozoic and Early Mesozoic tectono-thermal events in SE China. *Tectonophysics* **2011**, *501*, 71–86.
65. Shu, L.S.; Jahn, B.M.; Charvet, J.; Santosh, M.; Wang, B.; Xu, X.S.; Jiang, S.Y. Early Paleozoic depositional environment and intraplate tectono-magmatism in the Cathaysia block (South China): Evidence from stratigraphic, structural, geochemical and geochronological investigation. *Am. J. Sci.* **2014**, *314*, 154–186. [CrossRef]
66. Shu, L.S.; Yao, J.L.; Wang, B.; Faure, M.; Charvet, J.; Chen, Y. Neoproterozoic plate tectonic process and Phanerozoic geodynamic evolution of the South China Block. *Earth-Sci. Rev.* **2021**, *216*, 103596. [CrossRef]
67. Liu, H.; Zhao, X.L.; Jiang, J.; Zhang, J.G.; Liu, M.Z. The formation mechanism of the Xingguo vortex structure and its geological implication for the Mesozoic sinistral strike-slip in South China Block. *Chin. J. Geol.* **2021**, *56*, 808–828. (In Chinese with English abstract).
68. Zhang, J.K.; Cai, J.X. NE-SW-trending Hepu-Hetai dextral shear zone in southern China: Penetration of the Yunkai Promontory of South China into Indochina. *J. Struct. Geol.* **2009**, *31*, 737–748. [CrossRef]
69. Cai, J.X.; Zhang, J.K. A new model for the Indochina and South China collision during the Late Permian to the Middle Triassic. *Tectonophysics* **2009**, *467*, 35–43. [CrossRef]